

INERTIAL-NAVIGATION-SYSTEM AIDING BY COMBINING DATA LINK
AND SEEKER MEASUREMENTS

A THESIS SUBMITTED TO
THE GRADUATE SCHOOL OF NATURAL AND APPLIED SCIENCES
OF
MIDDLE EAST TECHNICAL UNIVERSITY

BY

EMRE HAN ATA

IN PARTIAL FULFILLMENT OF THE REQUIREMENTS
FOR
THE DEGREE OF MASTER OF SCIENCE
IN
MECHANICAL ENGINEERING

FEBRUARY 2022

Approval of the thesis:

**INERTIAL-NAVIGATION-SYSTEM AIDING BY COMBINING DATA
LINK AND SEEKER MEASUREMENTS**

submitted by **EMRE HAN ATA** in partial fulfillment of the requirements for the degree of **Master of Science in Mechanical Engineering, Middle East Technical University** by,

Prof. Dr. Halil Kalıpçılar
Dean, Graduate School of **Natural and Applied Sciences**

Prof. Dr. Sahir Arıkan
Head of the Department, **Mechanical Engineering**

Prof. Dr. Erhan İlhan Konukseven
Supervisor, **Mechanical Engineering Dept., METU**

Dr. Koray Savaş Erer
Co-Supervisor, **TMS-STD Dept., Roketsan Missile Inc.**

Examining Committee Members:

Prof. Dr. Kemal Leblebicioğlu
Electrical and Electronical Engineering Dept., METU

Prof. Dr. Erhan İlhan Konukseven
Mechanical Engineering Dept., METU

Assist. Prof. Dr. Ali Emre Turgut
Mechanical Engineering Dept., METU

Assoc. Prof. Dr. Bülent Özkan
Mechanical Engineering Dept., Gazi University

Assist. Prof. Dr. Ersin Söken
Aerospace Engineering Dept., METU

Date: 09.02.2022

I hereby declare that all information in this document has been obtained and presented in accordance with academic rules and ethical conduct. I also declare that, as required by these rules and conduct, I have fully cited and referenced all material and results that are not original to this work.

Name Last name : Emre Han Ata

Signature :

ABSTRACT

INERTIAL-NAVIGATION-SYSTEM AIDING BY COMBINING DATA LINK AND SEEKER MEASUREMENTS

Ata, Emre Han
Master of Science, Mechanical Engineering
Supervisor: Prof. Dr. Erhan İlhan Konukseven
Co-Supervisor: Dr. Koray Savaş Erer

February 2022, 87 pages

Missiles are equipped with seekers to increase the probability of intercepting the target. A gimballed seeker provides gimbal angles and rates used in a guidance law. Conventionally, the seeker is used at the terminal phase only. However, the seeker can also be used at the midcourse phase to eliminate inertial navigation system (INS) errors. Some missiles are also equipped with the data link to communicate with the platform. This data link provides data such as the image acquired by the seeker to the platform screen. The data link also offers range information between platform and missile, which can be used to increase the quality of INS solutions. In this thesis, a seeker and a data link are used to improve the INS solution. The INS errors are estimated by the Extended Kalman Filter (EKF). The attitude errors are not included in this study to make the system and analysis easier. Measurement models for the seeker gimbal angles and the data link range are derived. The proposed methodology does not require maneuver or the knowledge of the landmark position.

Keywords: INS Error Estimation, Extended Kalman Filter, Bearing-only Tracking, Data Link Range Measurement

ÖZ

VERİ BAĞI VE ARAYICI ÖLÇÜMLERİ İLE ATALETSEL- SEYRÜSEFER-SİSTEMİ DÜZELTMESİ

Ata, Emre Han
Yüksek Lisans, Makina Mühendisliği
Tez Yöneticisi: Prof. Dr. Erhan İlhan Konukseven
Ortak Tez Yöneticisi: Dr. Koray Savaş Erer

Şubat 2022, 87 sayfa

Vuruş kabiliyetini arttırmak amacıyla füzelere arayıcı takılmaktadır. Kardanlı arayıcıların sağladığı kardan açıları ve açısal hızları güdüm kanununda kullanılmaktadır. Geleneksel uygulamalarda arayıcı son safhada kullanılmaktadır. Oysaki arayıcı ara safhada ataletsel seyrüsefer sisteminin (ANS) hatalarını kapatmak için de kullanılabilir. Bazı füzelere veri bağı takılarak füze ile platform arasında iletişim sağlanmaktadır. Veri bağı arayıcı görüntüsü gibi verileri platform ekranına gönderir. Buna ek olarak veri bağı, füze ile platform arasındaki mesafeyi de ölçebilmektedir. Bu ölçüm de ANS hatalarını iyileştirmek için kullanılabilir. Bu tezde, arayıcı ve veri bağı kullanılarak seyrüsefer çözümü iyileştirilmiştir. Seyrüsefer hataları, Genişletilmiş Kalman Filtresi (GKF) ile kestirilmiştir. Sistem ve analizleri kolaylaştırması adına yönelim hataları çalışmaya dahil edilmemiştir. Ölçüm modeli, ölçüm denklemleri kullanılarak elde edilmiştir. Önerilen yöntem, füzenin manevra yapmasını ya da kilit atılan cismin konumunun bilinmesini gerektirmemektedir.

Anahtar Kelimeler: ANS Hata Kestirimi, Genişletilmiş Kalman Filtresi, Görüş Hattı Tabanlı Takip, Veri Bağı Mesafe Ölçümü

To my lovely wife

ACKNOWLEDGMENTS

I would like to express my gratitude to my supervisor Prof. Dr. Erhan İlhan Konukseven for providing an opportunity to work in the field of navigation, being supportive and understanding during my thesis work. I also would like to thank my co-supervisor Dr. Koray Savaş Erer for his brilliant ideas and guidance. I am so grateful that, this thesis study cannot be accomplished without him. I also wish to express my sincere thanks to my committee members for their contribution and comments on this study.

I would like to thank H. Ozan Ünsal for his invaluable technical insight he shared with me and my colleagues in Roketsan.

I also would like to thank Prof. Dr. M. Kemal Özgören and Dr. H. Ersin Söken for teaching me “Advanced Dynamics” and “Inertial Navigation Systems”; Prof. Dr. Ata Muğan and Dr. Merve Acer for their support at the beginning of this journey.

Above all, I would like to thank my family and friends for their endless love, encouragement and support.

Last but not the least important, I owe more than thanks to my dearest wife Nihan Ata for her endless love, patience, and support. Without her, this study would not have been even possible.

TABLE OF CONTENTS

ABSTRACT.....	v
ÖZ.....	vi
ACKNOWLEDGMENTS	viii
TABLE OF CONTENTS.....	ix
LIST OF TABLES	xi
LIST OF FIGURES	xii
LIST OF ABBREVIATIONS	xv
LIST OF SYMBOLS	xvi
CHAPTERS	
1 INTRODUCTION	1
1.1 Definition of the Problem	2
1.2 Literature Review.....	3
1.3 Contribution of the thesis.....	6
1.4 Outline.....	7
2 PROOF OF CONCEPT FOR POINT IN PLANE.....	9
2.1 Case 1: Only platform range is available	9
2.2 Case 2: Only landmark position and LOS are available	17
2.3 Case 3: Platform range and landmark LOS are available (proposed method)	21
3 3-D IMPLEMENTATION OF THE PROPOSED METHOD	29
3.1 Mathematical Details	29
3.1.1 System Model.....	29

3.1.2	Measurement Model	31
3.2	The Tuning and The Initialization of the Filter	32
4	SIMULATIONS AND DISCUSSIONS.....	37
4.1	Simulation and HWIL Test Scenario	38
4.2	Sensitivity to Errors	40
4.2.1	Sensitivity to Acceleration Errors.....	40
4.2.2	Sensitivity to Data Link and Seeker Measurement Errors.....	50
4.2.3	Sensitivity to Landmark Initialization	52
4.2.4	Realistic Monte Carlo Results	54
4.3	Hardware-In-The-Loop Test Results.....	57
5	CONCLUSION	65
	REFERENCES	67
	APPEDDICES	
A.	Extended Kalman Filter.....	71
B.	4-DOF Simulation	73
C.	Instrument Models.....	76
D.	Guidance Laws	80
E.	Investigating the Observability of “Case 2” and “Case 3”	82

LIST OF TABLES

TABLES

Table 1-1 Seeker Measurement Equations.....	4
Table 2-1 The EKF equations	12
Table 2-2 Errors used in the simulation	14
Table 4-1 Uniformly distributed initial INS errors for Monte Carlo runs and HWIL tests	39
Table 4-2 Accelerometer sensor specifications	40
Table 4-3 Datalink and seeker measurement errors used for testing sensitivity to accelerometer errors.....	41
Table 4-4 Datalink and seeker measurement errors for testing algorithm sensitivity to datalink and seeker measurement errors	50
Table 4-5 Datalink, seeker, and accelerometer errors and different landmark altitudes to test algorithm sensitivity to landmark initial error	52
Table 4-6 Measurement errors of HWIL testbed	59

LIST OF FIGURES

FIGURES

Figure 1-1 Missile subsystems	1
Figure 2-1 Single transmitter.....	10
Figure 2-2 Dual transmitters.....	10
Figure 2-3 Missile kinematics	13
Figure 2-4 2D-Planar trajectory of the missile	14
Figure 2-5 Position errors when only range is available	15
Figure 2-6 Velocity errors when only range is available	16
Figure 2-7 Bias errors when only range is available	16
Figure 2-8 LOS and LOS angle definitions.....	17
Figure 2-9 Position errors when only land mark position and LOS are available ..	19
Figure 2-10 Velocity errors when only land mark position and LOS are available	19
Figure 2-11 Bias errors when only land mark position and LOS are available	20
Figure 2-12 Position errors of the proposed method	22
Figure 2-13 Landmark position errors of the proposed method.....	23
Figure 2-14 Velocity errors of the proposed method	23
Figure 2-15 Bias errors of the proposed method	24
Figure 2-16 Zoomed view of Figure 2-14	24
Figure 2-17 Zoomed view of Figure 2-15	25
Figure 2-18 Position errors of three methods	26
Figure 2-19 Velocity errors of three methods	26
Figure 2-20 Bias errors of three methods	27
Figure 3-1 Kalman Filter behavior for varying P/R ratio [8]	33
Figure 3-2 Missile and landmark geometry.....	34
Figure 4-1 Platform trajectory, u-shape maneuver at the constant altitude.....	38
Figure 4-2 Missile trajectories in pitch and yaw planes	39
Figure 4-3 Missile position error for tactical-grade case.....	41
Figure 4-4 Missile velocity error for tactical-grade case.....	42

Figure 4-5 Landmark position error for tactical-grade case	42
Figure 4-6 Zoom view of Figure 4-4	43
Figure 4-7 RMSEs of position errors for EKF results and INS-only results (tactical-grade, 500 runs)	44
Figure 4-8 RMSEs of velocity errors for EKF results and INS-only results (tactical-grade, 500 runs)	45
Figure 4-9 RMSEs of the accelerometer bias errors (tactical-grade, 500 runs).....	45
Figure 4-10 Zoomed view of Figure 4-7.....	46
Figure 4-11 RMSEs of position errors for EKF results and INS-only results (consumer-grade, 500 runs)	47
Figure 4-12 RMSEs of velocity errors for EKF results and INS-only results (consumer -grade, 500 runs)	47
Figure 4-13 RMSEs of the accelerometer bias errors (consumer-grade, 500 runs)	48
Figure 4-14 Zoomed view of Figure 4-12.....	49
Figure 4-15 Zoomed view of Figure 4-13.....	49
Figure 4-16 RMSE of position for different cases	51
Figure 4-17 RMSE of velocity for different cases	51
Figure 4-18 RMSE of the missile position in terms of different landmark initial errors	53
Figure 4-19 RMSE of the missile velocity in terms of different landmark initial errors	53
Figure 4-20 RMSE of the missile position when all errors are at a realistic level..	54
Figure 4-21 RMSE of the missile velocity when all errors are at a realistic level..	55
Figure 4-22 RMSE of the bias when all errors are at a realistic level	55
Figure 4-23 Zoomed view of Figure 4-20.....	56
Figure 4-24 Zoomed view of Figure 4-21.....	57
Figure 4-25 3-axis FMS system [24]	58
Figure 4-26 5-axis FMS-TMS system [25].....	58
Figure 4-27 Acceleration command on body frame's y-z plane.....	59
Figure 4-28 Effect of the control gain, k , on the BTT performance	60

Figure 4-29 Calculated roll rates for different k values.....	60
Figure 4-30 Effect of the control gain, k, on the roll angle	61
Figure 4-31 BTT logic (Eq. (4.5))	61
Figure 4-32 Ideal case seeker scenes	62
Figure 4-33 INS-only case seeker scenes	62
Figure 4-34 INS aided case seeker scenes.....	62
Figure 4-35 Missile position errors	63
Figure 4-36 Missile velocity errors	63
Figure 4-37 Comparison of INS-only and EKF position errors	64
Figure 4-38 Comparison of INS-only and EKF velocity error.....	64

LIST OF ABBREVIATIONS

ABBREVIATIONS

BTT: Bank-to-Turn

CAS: Control Actuator System

DCM: Direction Cosine Matrix

DOF: Degree of Freedom

EKF: Extended Kalman Filter

FMS: Flight Motion Simulator

FOR: Field of Regard

GNSS: Global Navigation Satellite System

GPS: Global Positioning System

HWIL: Hardware in the Loop

IMU: Inertial Measurement Unit

INS: Inertial Navigation System

IIR: Imaging Infrared

LOS: Line of Sight

PNG: Proportional Navigation Guidance

RMSE: Root Mean Square Error

STT: Skid-to-Turn

TMA: Target Motion Analysis

TOF: Time of Flight

LIST OF SYMBOLS

SYMBOLS

x_m, y_m, z_m : Position of the missile

x_p, y_p, z_p : Position of the platform

x_L, y_L, z_L : Position of the landmark

v_x, v_y, v_z : Velocity of the missile

b_x, b_y, b_z : Bias of the accelerometer

a_x, a_y, a_z : Acceleration of the body

\bar{X} : States

\hat{F} : System matrix

\hat{B} : Input matrix

$\hat{\phi}_k$: Transition matrix at discrete time k

d_t : Time interval

$\hat{I}_{n \times n}$: n-by-n identity matrix

\hat{P}_k : Prediction covariance matrix

\hat{Q}_k : System noise matrix

\hat{R}_k : Measurement covariance matrix

\hat{K}_k : Kalman gain matrix

\hat{H} : Measurement matrix

λ_{el} : Gimbal elevation angle

λ_{az} : Gimbal azimuth angle

r : Data link range

η : White noise

$\hat{C}^{(\alpha,\beta)}$: DCM matrix from β frame to α frame

$\bar{u}_{\alpha\beta}^{(\gamma)}$: Column vector of unit vector of α -to- β , resolved in γ frame

ϕ, θ, ψ : Roll, pitch, yaw Euler angles

p, q, r : Body-angular velocity rates

\vec{a}_B : Body-acceleration vector

$\vec{\omega}_B$: Body-angular velocity vector

CHAPTER 1

INTRODUCTION

A guided missile can be defined as a munition that is directed towards a target by calculated steering commands. As shown in Figure 1-1, a missile consists of subsystems such as a control actuation system (CAS), navigation, guidance, autopilot, inertial measurement unit (IMU), and seeker.

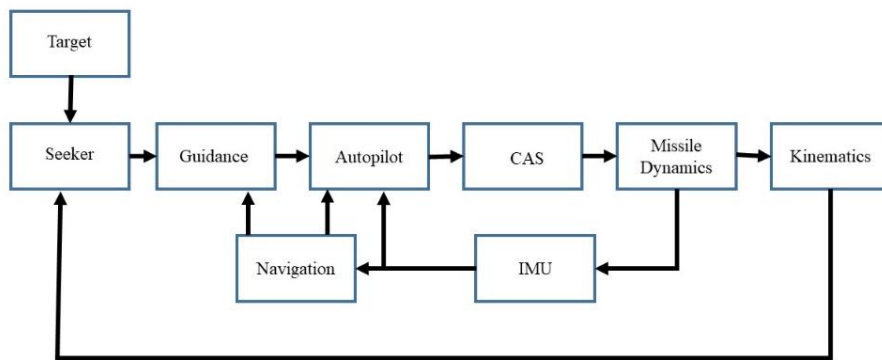


Figure 1-1 Missile subsystems

IMU consists of three accelerometers measuring translational acceleration and three gyroscopes measuring the angular velocity of the missile with respect to an inertial frame. The seeker is used to lock on the target to sense the relative motion of the target with respect to the missile. Navigation algorithms integrate IMU measurements to compute missile position, velocity, and attitude angles. Autopilot is responsible for the missile's stability and tracking the guidance commands. CAS is accountable for tracking autopilot's fin deflection commands. Guidance produces acceleration commands that direct the missile to the target. In the sense of guidance,

there are three phases for missile flight: the boost phase, mid-course, and terminal phase. Some missiles do not have boost and/or midcourse phases [6]. The boost phase is the phase where the missile rises to a predefined altitude. At the end of the midcourse, the missile is located somewhere to be able to lock on target. The terminal phase is the most critical phase. In this phase, the seeker and the navigation algorithms are used so that interception occurs.

1.1 Definition of the Problem

This study is motivated by navigation requirements in environments where a global navigation satellite system (GNSS) is unavailable. Global positioning system (GPS) is one of the most popular GNSSs. However, GPS signals might be blocked because of different sources, like signal jamming, receiver or satellite faults, missile dynamics (like missile's instant orientation can block the GPS antenna), etc. [8]. When the GPS signals are blocked, the INS solution diverges with time.

As mentioned before, the seeker is used to gather relative target motion with respect to the missile at the terminal phase. Seeker is generally not used before the terminal phase, but it can be used as an aiding sensor for navigation during the midcourse phase. Using seeker as an external aiding sensor for navigation, missile's costs could be reduced using cheaper IMU and removing the GPS antenna. In this study, seeker is assumed as imaging infrared (IIR) seeker.

Some missiles are also equipped with a data link, which transmits the image produced by the seeker from the missile to the platform; and commands from the platform to the missile. The transmission is done by radio waves. Besides transmitting data, the data link also measures the range between the missile and the platform. This range measurement makes it possible for the data link to be used as an external aiding sensor for navigation.

This study focuses on integrating seeker gimbal angles, datalink range, and inertial sensor measurements for robust, passive, and autonomous navigation systems. For

this purpose, an Extended Kalman Filter algorithm is applied. The proposed navigation system should be robust to the noises in the measurements and any external interferences. In addition, proposed method should be passive, which means that missile should not be detected.

1.2 Literature Review

Using seeker for INS aiding is not a new idea. Researchers have investigated and proposed different solutions.

[1] is one of the first studies conducted. Two modes are studied in this study. The first mode uses Line-of-Sight (LOS) angles, and the second mode uses the LOS rates as measurements. The seeker locks on the landmark during the midcourse phase. The position of the landmark is assumed to be known or estimated before. Two modes are used in the Extended Kalman Filter (EKF) to improve the 15-state INS error model solution.

In [2], the seeker is used to improve the INS solution during the midcourse. LOS angles and LOS rates are integrated with the INS by using the EKF. A 19-state INS error model is used. The states are three LOS-error, three velocity-error, three attitude-error, six IMU biases, two seeker gimbal potentiometer biases, and two seeker gimbal gyroscope biases as follows

$$\bar{X} = \begin{bmatrix} \delta r_{bL} \\ \delta V_m \\ \Delta\psi \\ b_g \\ b_a \\ b_p \\ b_{sg} \end{bmatrix} \quad (1)$$

where δr_{bL} is the error of the LOS vector from missile to landmark, δV_m , $\Delta\psi$ are velocity error and attitude error, b_g is gyroscope biases and b_a is accelerometer biases; b_p is seeker gimbal potentiometer biases, and b_{sg} is seeker gyroscope biases.

In [2], since the position of the landmark is not known, the position error of the missile is not compensated. On the other hand, the velocity error of the missile is compensated. The problem is formulated for flat-earth assumption, and the tuning and the initialization of the EKF is not implemented.

The study starts by formulating measurement equations: seeker gimbal angles, and LOS rates. After acquiring measurement equations, relations between measurement equations and states are obtained by using algebraic properties. When the relations are obtained, it is used in the EKF measurement equation.

The measurement equations are defined as follows

Table 1-1 Seeker Measurement Equations

$\lambda_{el} \doteq -\arctan\left(\frac{z_{mL}}{x_{mL}}\right)$	Seeker gimbal angles
$\lambda_{az} \doteq \arctan\left(\frac{y_{mL}}{\sqrt{(x_{mL})^2 + (z_{mL})^2}}\right)$	
$\vec{\omega}_{LOS} = \frac{\vec{v}_B \times \vec{r}_{mL}}{r_B^2}$	LOS angular rates

where λ_{el} , λ_{az} are elevation and azimuth seeker gimbal angles, respectively. x_{mL} , y_{mL} , z_{mL} are components of the LOS vector resolved in the body frame. $\vec{\omega}_{LOS}$ is LOS angular rates, \vec{v}_B is the relative velocity vector, and \vec{r}_{mL} is LOS vector from seeker to target. This measurement equations are valid for the 2-3 gimbal sequence.

Two critical phenomena are also considered in [2]. The first phenomenon is the ambiguity problem. As seen from the measurement equations (Table 1-1), if the relative position and velocity states are multiplied by same constant k, the same seeker gimbal angles and LOS rates are obtained. It is stated that the ambiguity problem is global, and the direction of the velocity is independent of the ambiguity.

The second important phenomenon mentioned is observability analysis. The observability analysis is performed using the observability matrix. Even though the

authors showed the observable and unobservable states, they do not explain why the states are observable or unobservable.

In [3], LOS angles provided by a two-axis gimbal system with yaw and pitch angles (3-2 sequence) are used to improve the INS solution by using indirect KF. For this purpose, indirect measurements are formed by the difference between raw and estimated measurements. The steps below are followed

1. Derive the unit LOS vector in navigation frame formed by the seeker measurement and attitude solution of the INS.
2. Derive the unit LOS vector in navigation frame formed by the known landmark position and position solution of the INS.
3. Subtract each other to get the indirect measurement.

It is seen that the indirect measurement is a function of position and the attitude solution of the INS, the position of the landmark, and measurement errors. The relation between the measurement and the states are used in the measurement equation of the EKF. A 15- state INS error model is augmented by two bias values of seeker sensors. In [3], GPS is also included in the KF architecture.

[4] uses LOS angles and radar altimeter to estimate INS errors of a cruise missile with the EKF. The seeker locks on a known landmark and tracks it to provide LOS angles. In [4], the missile is modeled as a point mass and, seeker and radar altimeter measurements compensate position and velocity errors. Since the system is modeled as a point, position and velocity are the only states in this study.

In [5], a 15-state INS error model is formulated, and the relationship between the INS error model and the LOS angles is built. A passive seeker locks on the known landmark and tracks it to provide the LOS angles. Like in [3], the calculated and measured LOS angles are used to improve the INS solution. For this purpose, Cramer-Rao lower bound is applied, and a sequential square root Kalman filter is designed.

In [7], image and inertial measurements are integrated to obtain navigation algorithm. This study assumes that the range from vehicle to the objects in the scene is available. This range is available since the binocular stereopsis is used, and the distance between two cameras is known. Also, landmark position is assumed to be known by using a statistical terrain model. The value is used for the initialization of the landmark position.

Aircrafts have more additional instruments than missiles to aid INS solution. In addition to seeker and data link, there are another devices used in aircrafts for INS aiding, such as altimeter, airspeed indicator, nondirectional radio beacon (NDB), very high frequency omni-directional range (VOR), very high frequency omni-directional range/tactical air navigation (VORTAC), long range navigation (LORAN) [31]. Usually, these devices are used to display indications located in the cockpit. The NDB uses low and medium frequency radio waves while the VOR exploits high frequency radio waves [31]. The devices that utilizes radio frequency to improve INS solution have the same features with data link.

Data link has become more popular with increase in the usage of unmanned aerial vehicles (UAV), and developments in the teconology. Data link is used for aircrafts, missiles, swarm robotics, communication, and formatin flight [32] [33].

1.3 Contribution of the thesis

The contribution of this thesis study is as follows:

- Position of the landmark is assumed to be known in the studies explained previously [1], [3], [4], [5], [7]. However, in this study, the position of the landmark is not needed with the help of the range provided by the data link. Also, this should be noted, the attitude of the missile is assumed to be known perfectly to make system and analysis easier. The INS uses accelerometer measurements to obtain the position and the velocity of the missile.

1.4 Outline

In chapter 2, the proposed concept is proven for a point in the plane. First of all, INS aiding results are discussed when only the platform range and the platform position are available. Then, INS aiding results are discussed when only the landmark position and LOS angle are available. Finally, the proposed methodology is discussed where INS is aided when platform position, platform range and land mark LOS angle are available.

In chapter 3, the 3-D implementation of the proposed concept is explained. For this purpose, mathematical details are given, and the tuning and the initializing procedure of the Kalman Filter is defined.

In chapter 4, the algorithm is tested in various conditions. Computer simulation results are given and discussed first, then hardware-in-the-loop (HWIL) application with a real IIR seeker on flight motion simulator (FMS) results are presented and discussed.

In chapter 5, the discussions of the thesis are concluded with the future works that could make the method better and more practical in real applications.

CHAPTER 2

PROOF OF CONCEPT FOR POINT IN PLANE

As mentioned in Chapter 1, two additional measurements, range from the data link and LOS angles from the seeker, are included to improve INS solutions. In this chapter, these measurements are investigated individually first. Then, integration of them is investigated. For simplicity, systems are modeled as a point in the plane. Three cases are investigated. In the first case, the range measurement from the data link and the accelerations from accelerometers are the only measurements. In the second case, the LOS angle from the seeker and the accelerations from accelerometers are the only measurements. Finally, in the third case, the proposed method, seeker, data link, and accelerometers are available simultaneously.

2.1 Case 1: Only platform range is available

The range is provided by the data link. Data link uses radio waves to communicate with the platform. The platform receives the image acquired by the seeker and transmits the commands and data such as the position of the platform. The range can be measured in different ways. Measuring the time of flight (TOF) is one of the most used methods [8]. Multiplying the TOF of the signal with the speed of light gives the range between the platform and the missile.

Obtaining the position of the receiver depends on the number of the available transmitters. For 2D-planar case, when there is only one transmitter, the receiver's position could be anywhere on the circle centered on the transmitter's position (see Figure 2-1).

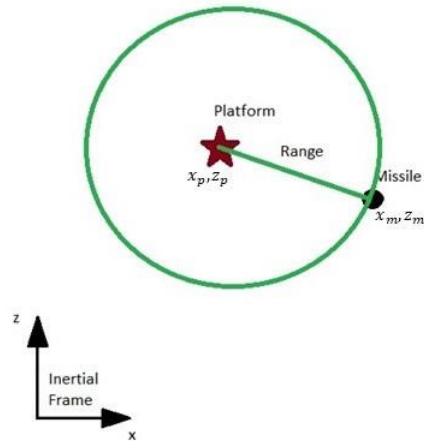


Figure 2-1 Single transmitter

As shown in Figure 2-2, when a second transmitter was added, the receiver could be on one of two intersection points. This ambiguity can be resolved by using a third transmitter or solving equations with constraints.

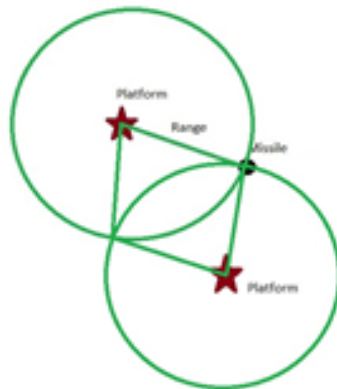


Figure 2-2 Dual transmitters

The range between transmitter and receiver (in our case, the transmitter is the platform, and the receiver is the missile) can be calculated by

$$r = \sqrt{(x_m - x_p)^2 + (z_m - z_p)^2} + \eta_r \quad (2.1)$$

where, x_m, z_m are the position of the missile, and x_p, z_p are the position of the platform, and η_r is an uncorrelated, zero-mean additive Gaussian noise where $\eta_r \sim N(0, \sigma_r)$.

The EKF requires linear or linearized measurement matrix. Since this measurement equation is nonlinear, a linear relationship between measurement and the missile position should be obtained. Eq. (2.1) can be linearized by taking derivatives of the equation with respect to the missile position. Jacobian matrix of the related equation can be given by

$$\partial r = \begin{bmatrix} \frac{x_m - x_p}{r} & \frac{z_m - z_p}{r} \end{bmatrix} \begin{bmatrix} \partial x_m \\ \partial z_m \end{bmatrix} \quad (2.2)$$

This relation can be used in an EKF. A 6-state EKF can be used as the states are given below

$$X = \begin{bmatrix} x_m \\ z_m \\ v_x \\ v_z \\ b_x \\ b_z \end{bmatrix} \quad (2.3)$$

The system equations can be written as

$$\begin{bmatrix} \dot{x}_m \\ \dot{z}_m \\ \dot{v}_x \\ \dot{v}_z \\ \dot{b}_x \\ \dot{b}_z \end{bmatrix} = \begin{bmatrix} 0 & 0 & 1 & 0 & 0 & 0 \\ 0 & 0 & 0 & 1 & 0 & 0 \\ 0 & 0 & 0 & 0 & -1 & 0 \\ 0 & 0 & 0 & 0 & 0 & -1 \\ 0 & 0 & 0 & 0 & 0 & 0 \\ 0 & 0 & 0 & 0 & 0 & 0 \end{bmatrix} \begin{bmatrix} x_m \\ z_m \\ v_x \\ v_z \\ b_x \\ b_z \end{bmatrix} + \begin{bmatrix} 0 & 0 \\ 0 & 0 \\ 1 & 0 \\ 0 & 1 \\ 0 & 0 \\ 0 & 0 \end{bmatrix} \begin{bmatrix} a_x \\ a_z \end{bmatrix} \quad (2.4)$$

$$\dot{\hat{X}} = \hat{F}\hat{X} + \hat{B}\hat{a}_m^{(i)}$$

where, x_m, z_m are the horizontal and the vertical positions of the missile, v_x, v_z are the horizontal and the vertical speeds of the missile, b_x, b_z are biases of the

accelerometer, which are modeled as constants, and a_x, a_z are accelerations of the missile measured by the accelerometer in the inertial frame. The accelerometer is assumed not to be strapdown but perfectly stabilized in order to measure accelerations in the inertial frame. This assumption makes system equations simpler.

The continuous system model can be expressed as discrete form as follows [10]

$$\bar{X}_{k+1} = \hat{\Phi}_k \bar{X}_k + \hat{B}_k \bar{a}_m^{(i)} \quad (2.5)$$

where system transition matrix, $\hat{\Phi}_k$, can be obtained by Taylor expression of \hat{F} matrix with neglecting higher-order terms as follows

$$\hat{\Phi}_k = \hat{I}_{6 \times 6} + \hat{F} d_t \quad (2.6)$$

where d_t is the time interval, and $\hat{I}_{6 \times 6}$ is the identity matrix.

Also, \hat{B}_k can be written as

$$\hat{B}_k = \hat{B} d_t \quad (2.7)$$

The Extended Kalman Filter (EKF) equations of the given system can be summarized as (see Appendix-A)

Table 2-1 The EKF equations

Time update	$\bar{X}_{k+1/k} = \hat{\Phi}_k \bar{X}_{k/k} + \hat{B}_k \bar{a}_m^{(i)}$ $\hat{P}_{k+1/k} = \hat{\Phi}_k \hat{P}_{k/k} \hat{\Phi}_k^T + \hat{Q}_k$
Measurement update	$\hat{K}_k = \hat{P}_{k+1/k} \hat{H}_k^T (\hat{H}_k \hat{P}_{k+1/k} \hat{H}_k^T + \hat{R}_k)^{-1}$ $\hat{P}_{k+1/k+1} = (\hat{I} - \hat{K}_k \hat{H}_k) \hat{P}_{k+1/k}$ $\bar{X}_{k+1/k+1} = \bar{X}_{k+1/k} + \hat{K}_k (\bar{r}_m - \bar{r}_{INS})$

where $\hat{P}_{k+1/k}$ and \hat{R}_k are the prediction covariance matrix and the measurement covariance matrix, respectively. The details of choosing the covariance matrices are explained later in this section. \hat{H} is the Jacobian matrix form of the measurement equation, and \bar{r}_{INS} is calculated from INS solution. \hat{K}_k is the Kalman gains matrix.

\hat{H} matrix is the Jacobian of the measurement equation and can be written by using Eq. (2.2) as

$$\hat{H} = \begin{bmatrix} \frac{x_m - x_p}{r} & \frac{z_m - z_p}{r} & 0 & 0 & 0 & 0 \end{bmatrix} \quad (2.8)$$

where x_m and z_m are horizontal and vertical position of the missile and obtained by the INS solution. x_p and z_p are horizontal and vertical position of the platform and provided by the data link.

2-D simulation is run to evaluate the performance of the method. Missile is released from the platform with 250 m/s initial velocity in the x-axis and 3000 m above the target. Target is located at the 10000 m in the x-axis. The missile approaches to the target with Proportional Navigation Guidance (PNG), and the navigation gain is selected as 3. The guidance loop is completed by true position and velocity of the missile. The details of the PNG law are shared in Appendix-D. The platform is assumed to be stationary and located at the origin. Missile's position and velocity are obtained by integrating acceleration command generated by the PNG as shown in Figure 2-3. Missile dynamics is omitted, which means there is no autopilot or CAS delays.

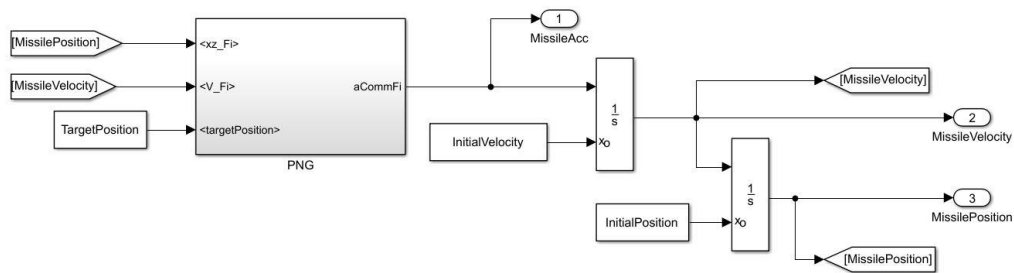


Figure 2-3 Missile kinematics

The trajectory of the missile, the position of the platform and the target are shown in Figure 2-4.

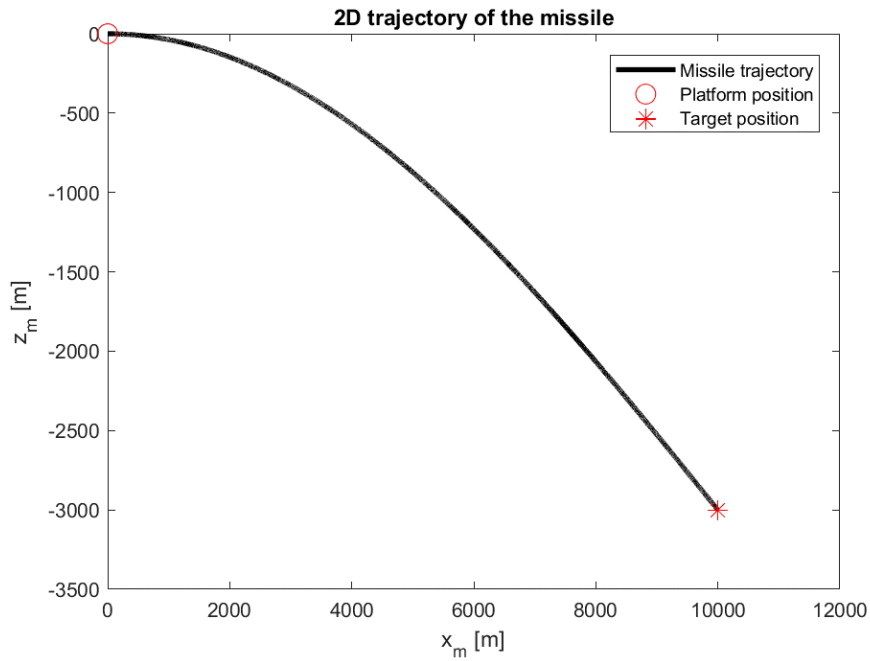


Figure 2-4 2D-Planar trajectory of the missile

Initial INS errors and the measurement errors are as follows:

Table 2-2 Errors used in the simulation

Parameters	Errors
Initial Position errors	[-50;20] m
Initial Velocity errors	[-5;2] m/s
Initial Bias errors	[0.3;0.3] m/s ²
Data link range standard deviation (1σ)	1 m
Accelerometer Biases	[0.1;0.1] m/s ²
Accelerometer standard deviation (1σ)	[0.01;0.01] m/s ²

Tunable EKF parameters are selected as follows:

- P_0 is selected as $\text{diag}([100 \ 100 \ 10 \ 10 \ 0.6 \ 0.6].^2)$. Components of the P_0 are the square of the twice of the maximum initial error (see Table 2-2).

- R_k is selected according to the corresponding measurement error. In this simulation, it is chosen as 4, the square of twice standard deviation of the range error.
- Velocity state relevant elements of Q_k are selected as 0.004, the square of twice standard deviation of the accelerometer errors. The values for other states are selected as zero.

The results are shown below. Figure 2-5 shows the position error of the EKF. Upper and lower boundaries are the covariance of the corresponding state. Figure 2-6 shows the velocity error of the EKF. Figure 2-7 shows the bias errors of the accelerometer. Bias errors are calculated by subtracting the estimated bias values from the actual bias values.

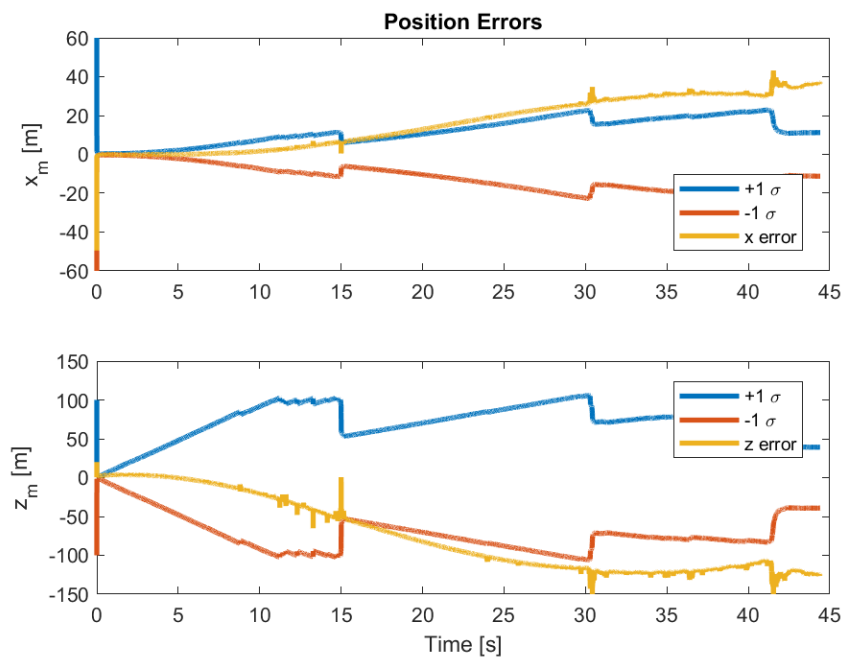


Figure 2-5 Position errors when only range is available

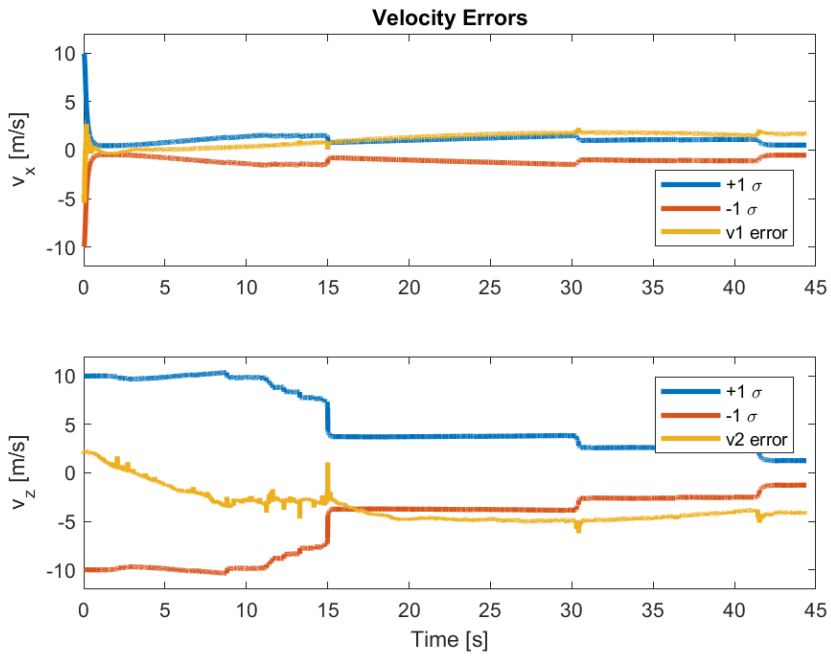


Figure 2-6 Velocity errors when only range is available

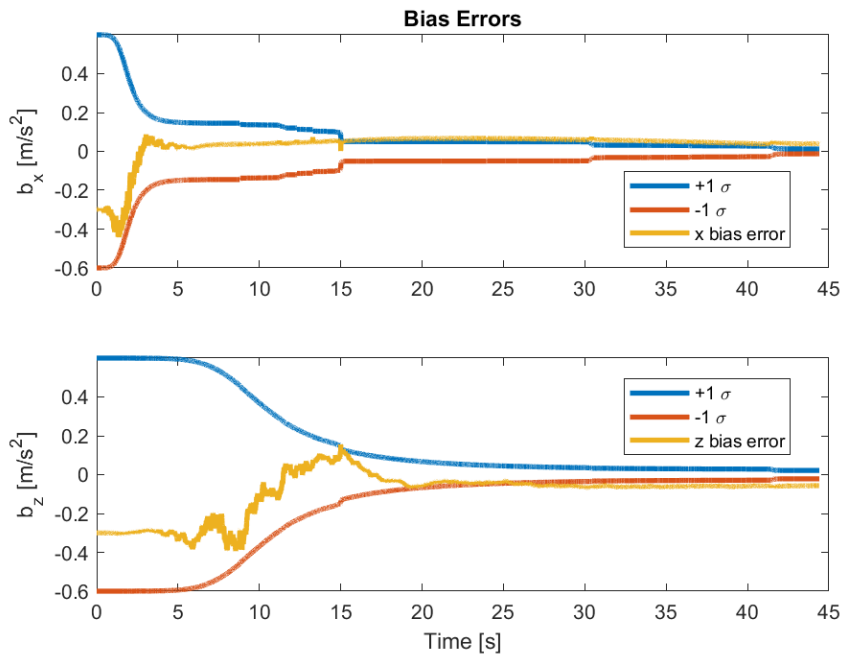


Figure 2-7 Bias errors when only range is available

Figure 2-5, Figure 2-6, and Figure 2-7 show that INS states cannot be fully compensated. The covariance boundaries do not decrease, which indicates the

uncertainty in the solution does not decrease. This is expected since this is the same case with a single transmitter and a single receiver in a plane [8].

2.2 Case 2: Only landmark position and LOS are available

The LOS angle is provided by the IIR seeker in this thesis. IIR seekers are classified as passive seekers, which use energy emitted by the target in the IR spectrum [9]. LOS angle is defined as the angle between the LOS vector, which is the line from seeker to target, and the nonrotating reference line (inertial ground) as shown below [6].

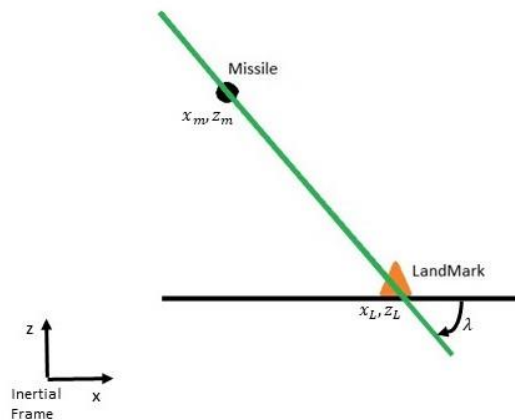


Figure 2-8 LOS and LOS angle definitions

The assumptions made for the seeker model is listed as follows:

- Gimbal only provides the LOS angle.
- Lock-on range (LOR) of the seeker is not specified.
- Limited field of regard (FOR) is not considered.
- Ideal tracking of the seeker is assumed, which means there is no delay.
- The gimbal dynamics are omitted.

LOS angle can be calculated by

$$\lambda = \arctan\left(\frac{z_L - z_m}{x_L - x_m}\right) + \eta_\lambda \quad (2.9)$$

where x_L and z_L are the position of the landmark, it is assumed to be known. η_λ is an uncorrelated, zero-mean additive Gaussian noise where $\eta_\lambda \sim N(0, \sigma_\lambda)$.

Since this measurement equation is nonlinear, and the EKF requires a linear or linearized measurement model, a linear relationship between measurement and the missile position should be obtained. Eq. (2.9) can be linearized by taking derivatives of the equation with respect to the missile position. Jacobian matrix of the related measurement equation can be given by

$$\lambda = \begin{bmatrix} \frac{z_L - z_m}{R_L^2} & -\frac{x_L - x_m}{R_L^2} \end{bmatrix} \begin{bmatrix} \partial x_m \\ \partial z_m \end{bmatrix} \quad (2.10)$$

where

$$R_L^2 = (x_L - x_m)^2 + (z_L - z_m)^2 \quad (2.11)$$

The Eq. 2.11 can be used in the EKF given in Table 2-1. The Same system equations (Eq. (2.3) – (2.7)) of case 1 can be used. The only difference is the measurement Jacobian matrix, and it can be written by using Eq. (2.10) as

$$\hat{H} = \begin{bmatrix} \frac{z_L - z_m}{R_L^2} & -\frac{x_L - x_m}{R_L^2} & 0 & 0 & 0 & 0 \end{bmatrix} \quad (2.12)$$

2-D simulation is conducted to evaluate the performance of the method. In addition to the scenario given in Section 2.1, there is a landmark located at the target. Tunable EKF parameters are selected as the same with case 1 except for the measurement covariance. \hat{R}_k is chosen as the square of twice the standard deviation of the measurement error.

2-D simulation results are shown below.

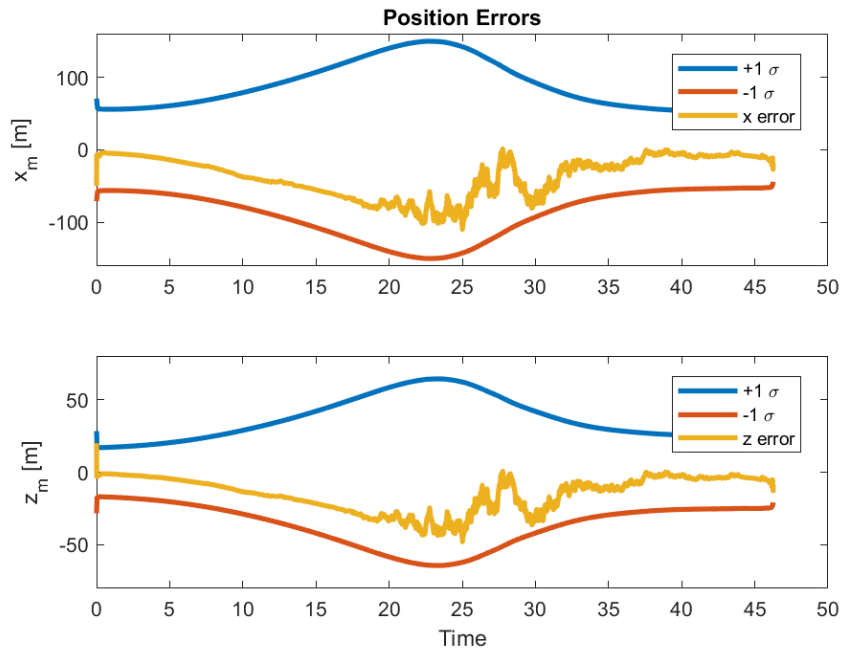


Figure 2-9 Position errors when only land mark position and LOS are available

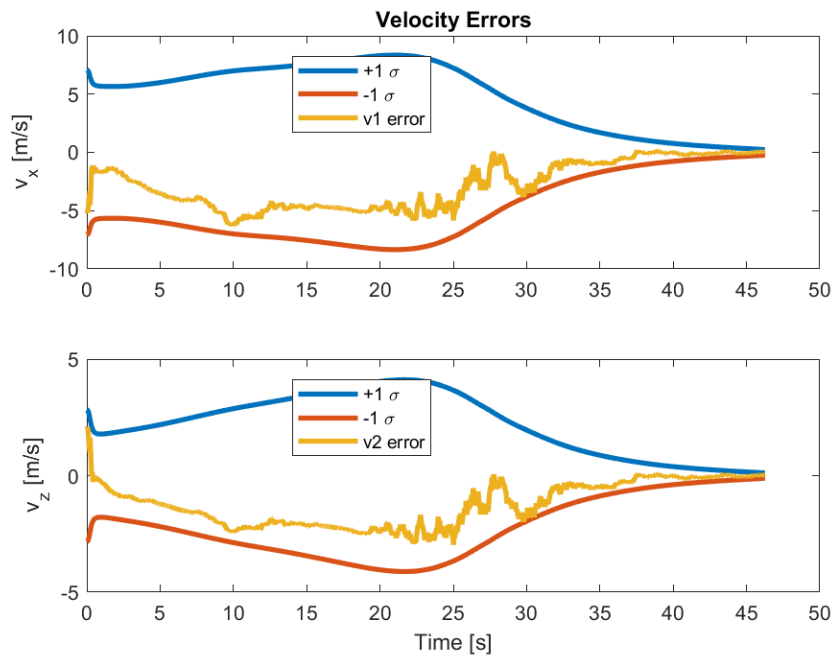


Figure 2-10 Velocity errors when only land mark position and LOS are available

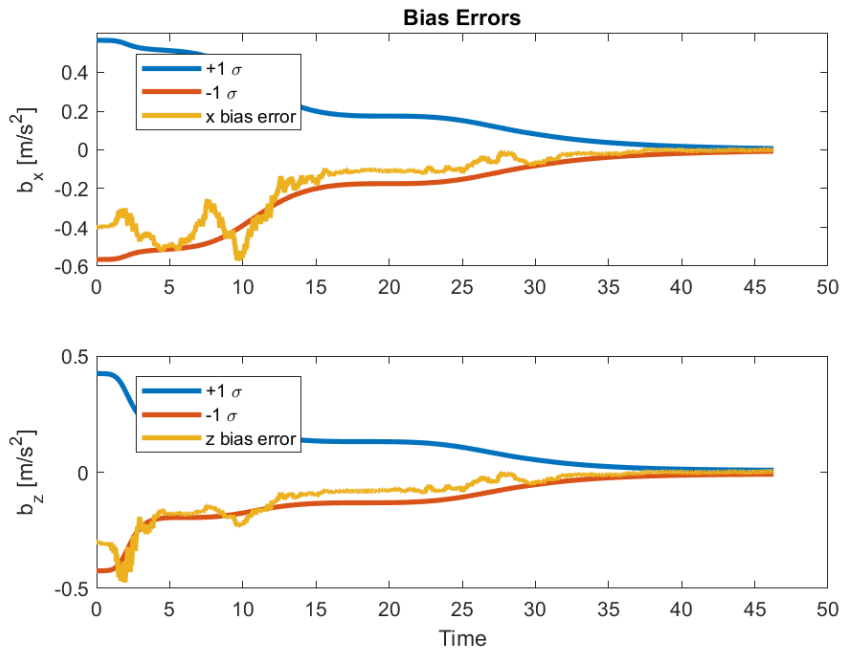


Figure 2-11 Bias errors when only land mark position and LOS are available

These results are same with the literature [1], [3], [4], [5], [7]. In case of landmark position is known, INS errors can be compensated by only using tracking angle. Even though it is not necessary to maneuver, some studies suggested maneuvering to increase observability. For instance, [3] used S-maneuver to increase observability.

At the beginning of the filter, covariance values of the position states increases. After around 25 seconds, covariances starts decreasing. The reason of this behaviour is highly related to the filter observability. As mention in Appendix-E, filter observability depends on LOS rate existance. At the beginning of the filter, target is far away from the missile causing low-LOS rate values, which is the reason of the increasing covariance boundaries. The observability of the states are investigated in Appendix-E.

2.3 Case 3: Platform range and landmark LOS are available (proposed method)

As explained before, using only the range from the platform with the known position is not enough to improve INS errors. On the other hand, using only the LOS angle to the landmark is enough, but the position of the landmark is supposed to be known, which is an essential restriction for real applications. In this study, it is proposed that platform range and the land mark LOS can be used to improve INS errors without requiring the position of the landmark.

Since the position of the landmark is unknown and is desired to be estimated, the position of the landmark is also added to the states. In this case, states of the filter would be as follows

$$\bar{X} = \begin{bmatrix} x_m \\ z_m \\ v_x \\ v_z \\ b_x \\ b_z \\ x_L \\ z_L \end{bmatrix} \quad (2.19)$$

Continuous system equations can be re-written by assuming the position of the landmark is fixed as

$$\begin{bmatrix} \dot{x}_m \\ \dot{z}_m \\ \dot{v}_x \\ \dot{v}_z \\ \dot{b}_x \\ \dot{b}_z \\ \dot{x}_L \\ \dot{z}_L \end{bmatrix} = \begin{bmatrix} 0 & 0 & 1 & 0 & 0 & 0 & 0 & 0 \\ 0 & 0 & 0 & 1 & 0 & 0 & 0 & 0 \\ 0 & 0 & 0 & 0 & -1 & 0 & 0 & 0 \\ 0 & 0 & 0 & 0 & 0 & -1 & 0 & 0 \\ 0 & 0 & 0 & 0 & 0 & 0 & 0 & 0 \\ 0 & 0 & 0 & 0 & 0 & 0 & 0 & 0 \\ 0 & 0 & 0 & 0 & 0 & 0 & 0 & 0 \\ 0 & 0 & 0 & 0 & 0 & 0 & 0 & 0 \end{bmatrix} \begin{bmatrix} x_m \\ z_m \\ v_x \\ v_z \\ b_x \\ b_z \\ x_L \\ z_L \end{bmatrix} + \begin{bmatrix} 0 & 0 \\ 0 & 0 \\ 1 & 0 \\ 0 & 1 \\ 0 & 0 \\ 0 & 0 \\ 0 & 0 \\ 0 & 0 \end{bmatrix} \begin{bmatrix} a_x \\ a_z \end{bmatrix} \quad (2.20)$$

The discrete form can be obtained by using the same procedure done before, Eq. (2-5) – (2.7). Measurement matrices given by Eq. (2.2) and Eq. (2.10) can be merged as follows

$$\begin{bmatrix} \partial r \\ \partial \lambda \end{bmatrix} = \begin{bmatrix} \frac{x_m - x_p}{r} & \frac{z_m - z_p}{r} & 0 & 0 & 0 & 0 & 0 & 0 \\ \frac{z_L - z_m}{R_L^2} & -\frac{x_L - x_m}{R_L^2} & 0 & 0 & 0 & 0 & -\frac{z_L - z_m}{R_L^2} & \frac{x_L - x_m}{R_L^2} \end{bmatrix} \begin{bmatrix} \partial x_m \\ \partial z_m \\ \partial v_x \\ \partial v_z \\ \partial b_x \\ \partial b_z \\ \partial x_L \\ \partial z_L \end{bmatrix} \quad (2.21)$$

2-D simulation is run to evaluate the performance of the proposed method. The scenario is same with the ones used in Section 2.1 and Section 2.2. In addition, landmark position state relevant elements of Q_k is selected as zero.

The results for the proposed method are shown below. Figure 2-12 shows the position error of the EKF results. Figure 2-13 shows landmark position error, which is calculated by subtracting the estimated landmark position from the actual landmark position. The same phenomenon about the observability is also shown in proposed method. At the beginning of the filter, the covariance of the position states increases.

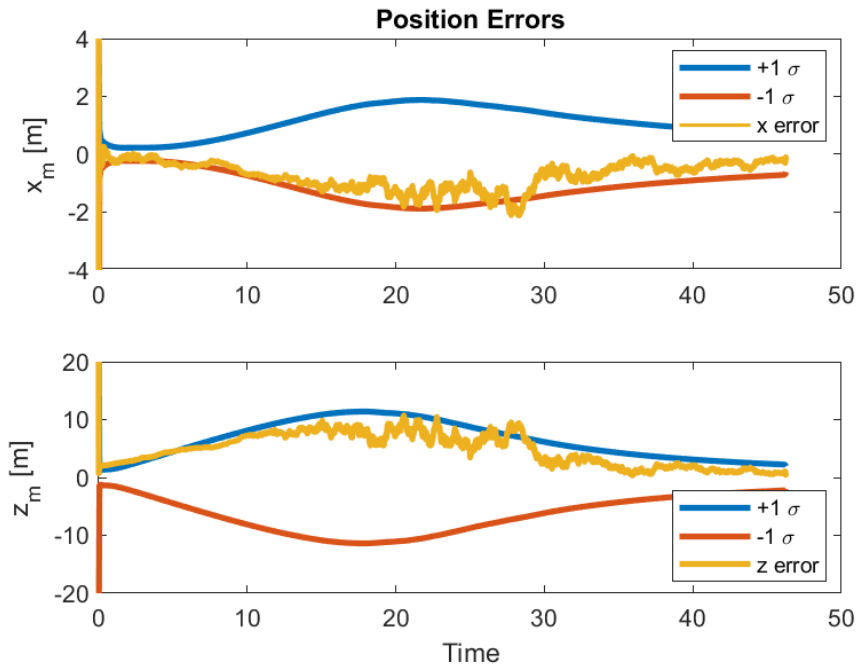


Figure 2-12 Position errors of the proposed method

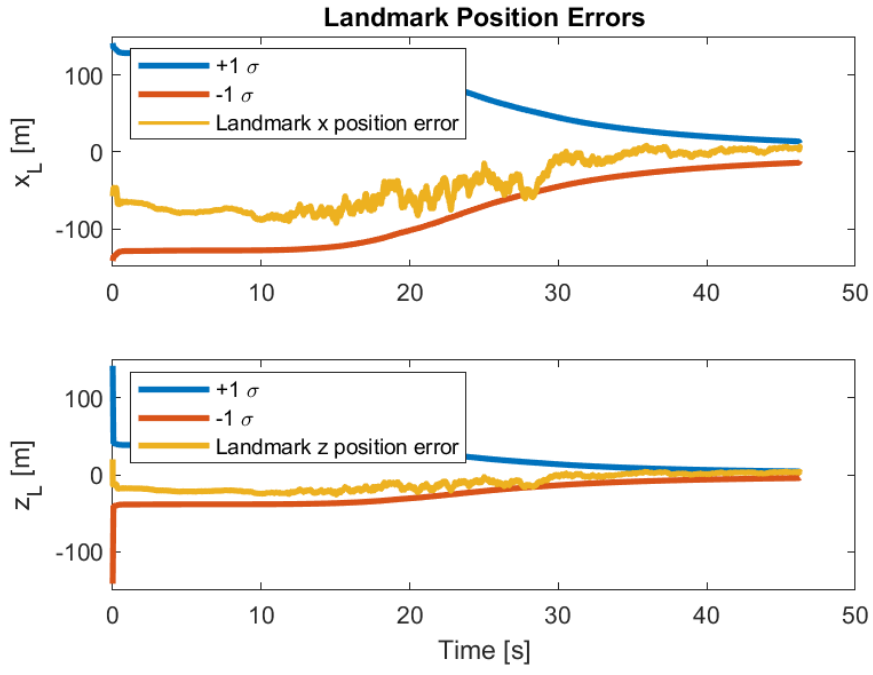


Figure 2-13 Landmark position errors of the proposed method

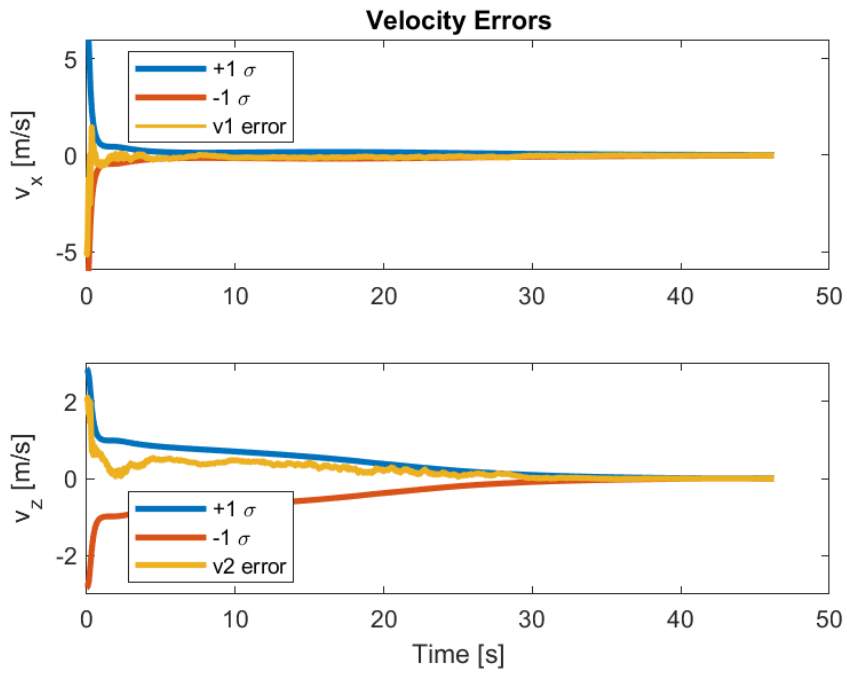


Figure 2-14 Velocity errors of the proposed method

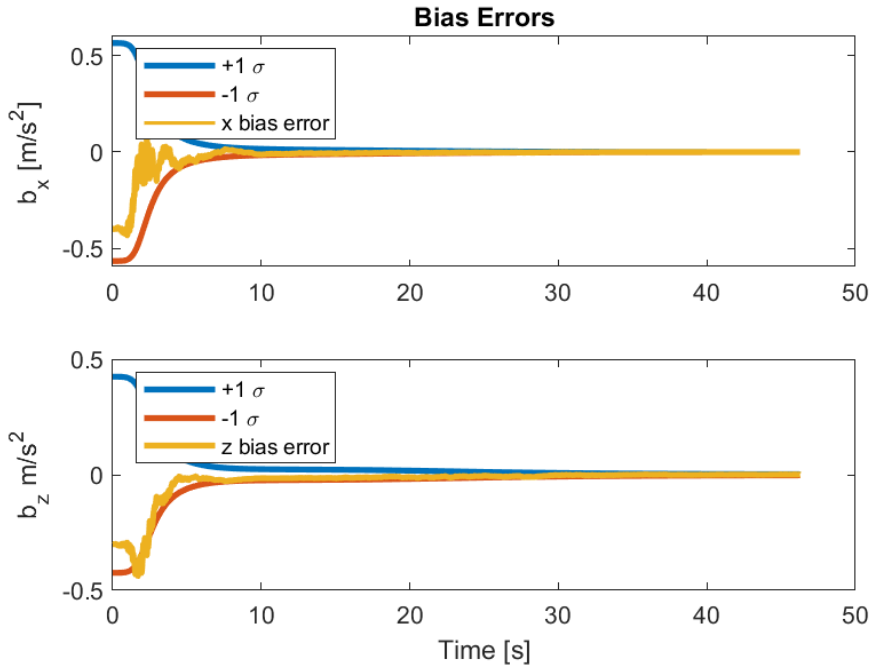


Figure 2-15 Bias errors of the proposed method

Zoomed view of Figure 2-14 and Figure 2-15 are shown below. As seen from figures, errors are always within covariance boundaries.

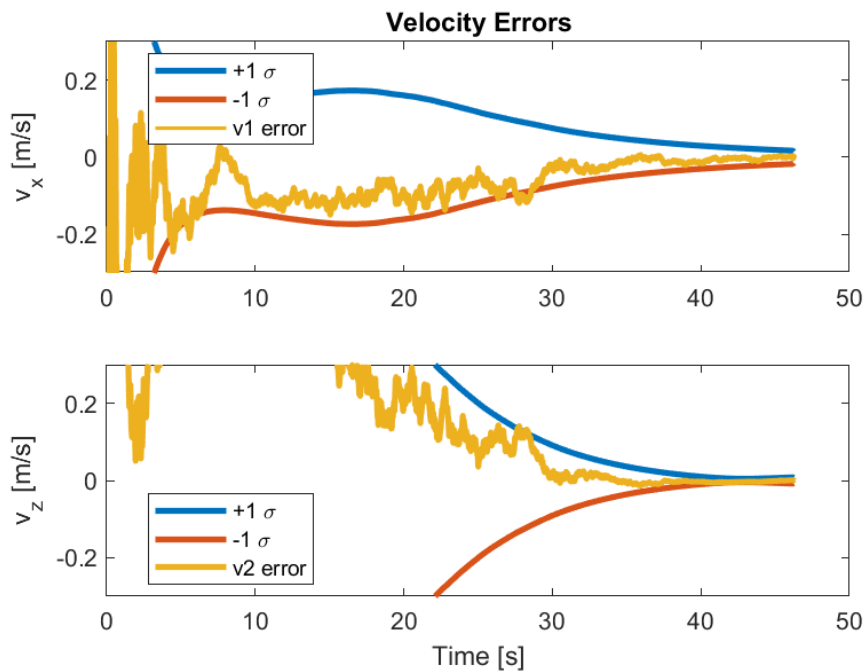


Figure 2-16 Zoomed view of Figure 2-14

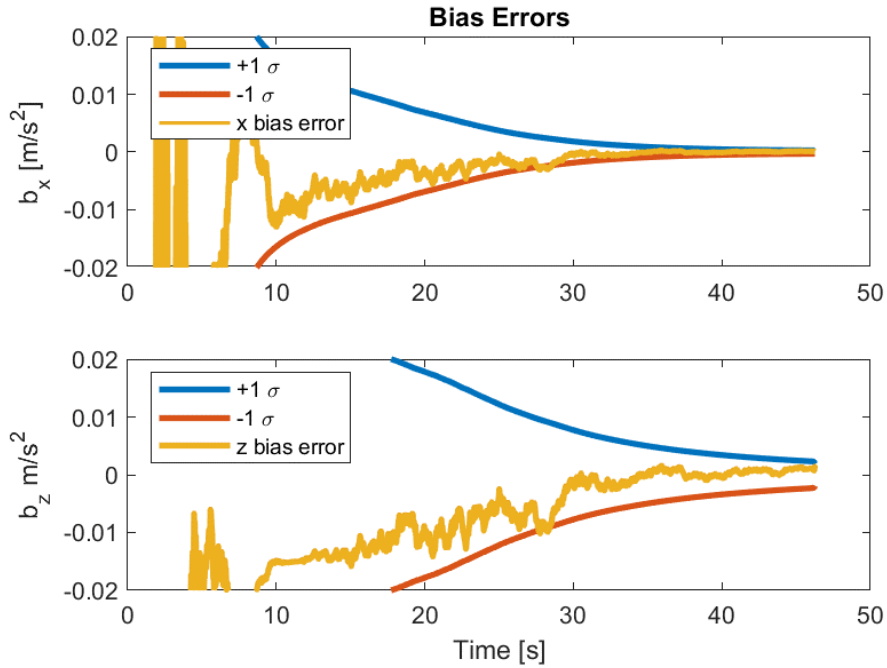


Figure 2-17 Zoomed view of Figure 2-15

INS errors are well estimated, as it can be seen from figures. To compare three methods given above, errors are drawn in the same figure. Figure 2-18 shows the position errors of the three methods. Proposed method shows superior performance. It converges zero with higher rate, and keeps errors low. Figure 2-19 and Figure 2-20 show the velocity and the bias errors of the three methods, respectively.

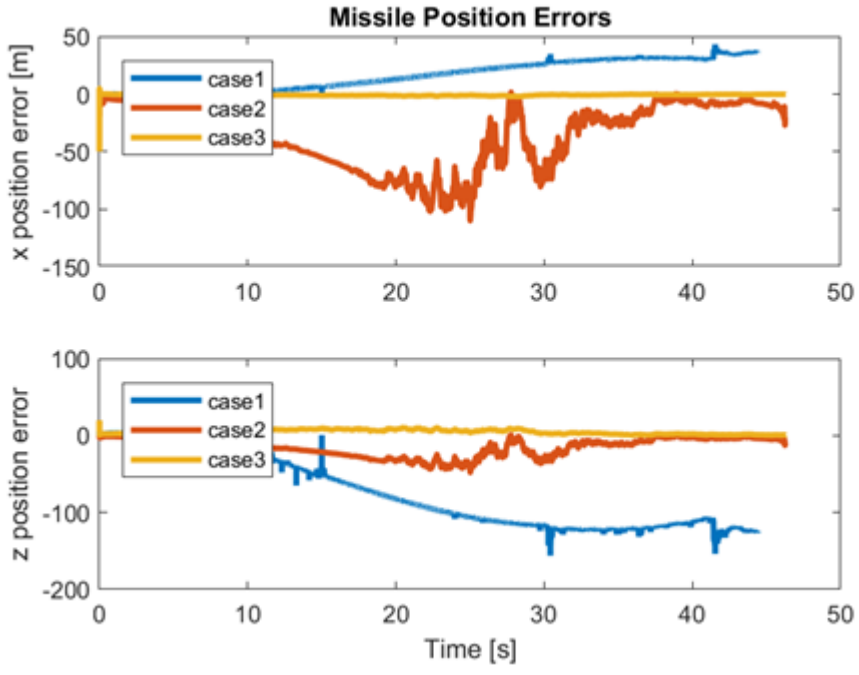


Figure 2-18 Position errors of three methods

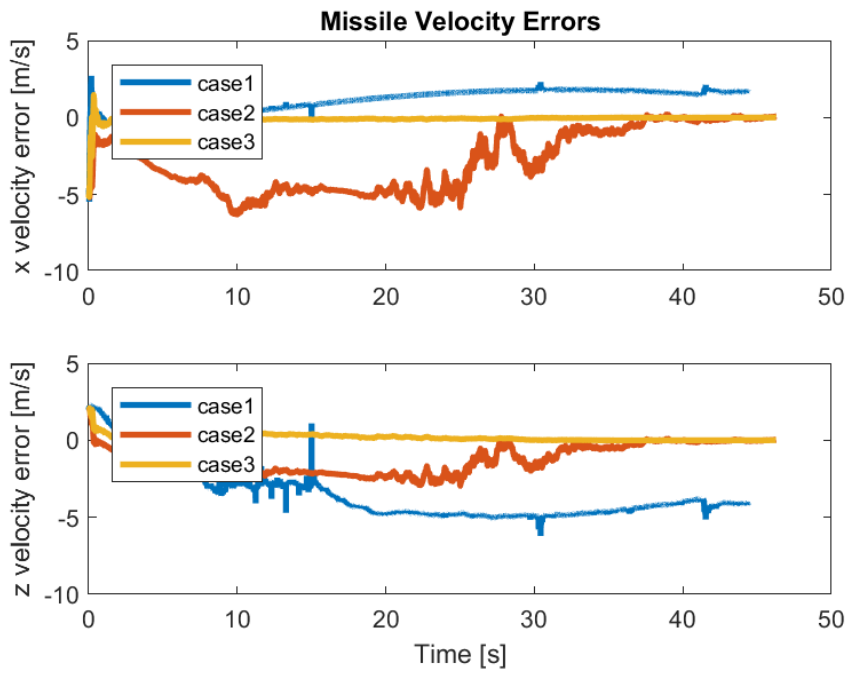


Figure 2-19 Velocity errors of three methods

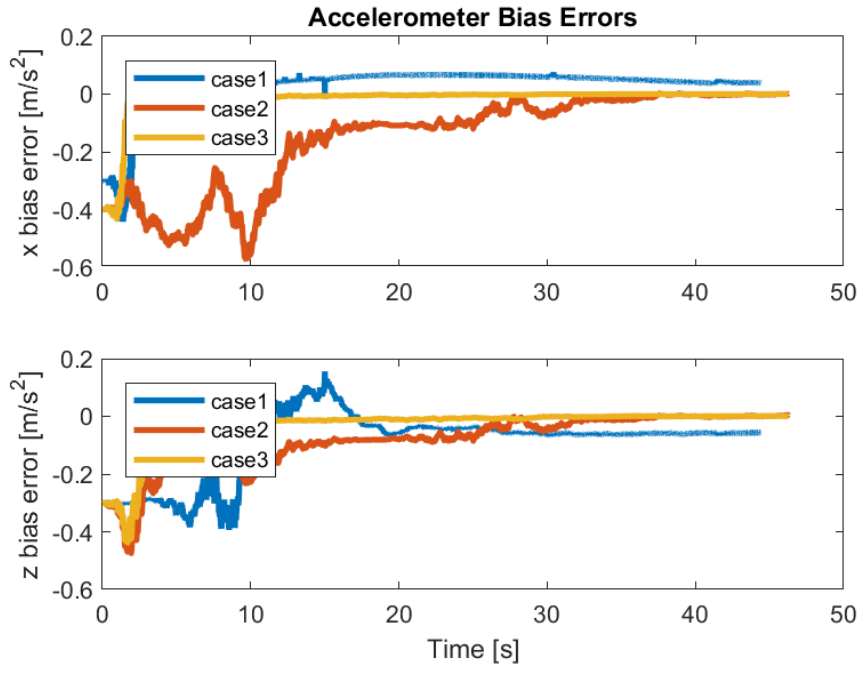


Figure 2-20 Bias errors of three methods

CHAPTER 3

3-D IMPLEMENTATION OF THE PROPOSED METHOD

In this chapter, 3-D implementation of the proposed method is conducted. In Chapter 2, system is modeled by nominal states, and there are only two measurements: range from datalink and LOS angle from gimballed seeker. Also, platform was modeled as stationary at the origin. On the other hand, in this chapter the platform is assumed to be a vehicle carrying the missile, such as a fighter aircraft. In some real applications, after platform releases the missile, it turns and goes away to avoid opponent's defence systems. Instead of nominal states, error-states are used. Also, there are three measurements: range from data link and two LOS angles (pitch and yaw) from gimballed seeker.

3.1 Mathematical Details

3.1.1 System Model

In chapter 2, nominal states are used. Nominal states are valid for the system in this study, since the attitude is excluded from INS states. On the other hand, when the attitude is included, error states should be utilized to obtain linear system model [30]. In this chapter, error states are used to make it easier for the future studies when the attitude and gyroscope errors are included.

States used in the previous chapter can be extended to 3D as error states as follows

$$\bar{X} = \begin{bmatrix} \delta x \\ \delta y \\ \delta z \\ \delta v_1 \\ \delta v_2 \\ \delta v_3 \\ b_x \\ b_y \\ b_z \\ \delta x_L \\ \delta y_L \\ \delta z_L \end{bmatrix} \quad (3.1)$$

Continuous system equations can be written as

$$\begin{bmatrix} \delta \dot{x}_m \\ \delta \dot{y}_m \\ \delta \dot{z}_m \\ \delta \dot{v}_x \\ \delta \dot{v}_y \\ \delta \dot{v}_z \\ \dot{b}_x \\ \dot{b}_y \\ \dot{b}_z \\ \delta \dot{x}_L \\ \delta \dot{y}_L \\ \delta \dot{z}_L \end{bmatrix} = \begin{bmatrix} \hat{0}_{3 \times 3} & \hat{I}_{3 \times 3} & \hat{0}_{3 \times 3} & \hat{0}_{3 \times 3} & \hat{0}_{3 \times 3} \\ \hat{0}_{3 \times 3} & \hat{0}_{3 \times 3} & \hat{C}^{(i,b)} & \hat{0}_{3 \times 3} & \hat{0}_{3 \times 3} \\ \hat{0}_{3 \times 3} & \hat{0}_{3 \times 3} & \hat{0}_{3 \times 3} & \hat{0}_{3 \times 3} & \hat{0}_{3 \times 3} \\ \hat{0}_{3 \times 3} & \hat{0}_{3 \times 3} & \hat{0}_{3 \times 3} & \hat{0}_{3 \times 3} & \hat{0}_{3 \times 3} \end{bmatrix} \begin{bmatrix} \delta x_m \\ \delta y_m \\ \delta z_m \\ \delta v_x \\ \delta v_y \\ \delta v_z \\ b_x \\ b_y \\ b_z \\ \delta x_L \\ \delta y_L \\ \delta z_L \end{bmatrix} \quad (3.2)$$

$$\dot{\bar{X}} = \hat{F} \bar{X}$$

where $\delta x_m, \delta y_m, \delta z_m$ are position error terms of the missile, $\delta v_x, \delta v_y, \delta v_z$ are the velocity error terms of the missile, b_x, b_y, b_z are the bias terms of the accelerometer, and $\delta x_L, \delta y_L, \delta z_L$ are the position error terms of the landmark.

Assumption: The DCM from the body frame to the inertial frame, $\hat{C}^{(i,b)}$, is assumed to be known.

Discrete form of the system can be obtained by

$$\bar{X}_{k+1} = \hat{\Phi}_k \bar{X}_k \quad (3.3)$$

where system transition matrix, $\hat{\Phi}_k$, can be obtained by Taylor expression of \hat{F} matrix with neglecting higher order terms as done in Section 2.1.

This system model will be used in the EKF after relation between measurements and the states are obtained.

3.1.2 Measurement Model

Datalink Measurement Equation can be written in 3D as follows

$$r = \sqrt{(x_m - x_p)^2 + (y_m - y_p)^2 + (z_m - z_p)^2} + \eta_r \quad (3.4)$$

where, x_m, y_m, z_m are position of the missile, and x_p, y_p, z_p are position of the platform, and η_r is an uncorrelated, zero mean additive Gaussian noise where $\eta_r \sim N(0, \sigma_r)$.

Normally, the seeker measures the gimbal angles which provides the angular position of the land mark with respect to the body frame. However, since we assume DCM from the body frame to the inertial frame is known, the seeker is said to measure LOS angle. The seeker measurements can be written as

$$\lambda_{az} = \text{atan}_2\left(\frac{y_L - y_m}{x_L - x_m}\right) + \eta_\lambda \quad (3.5)$$

$$\lambda_{el} = \text{atan}_2\left(\frac{z_L - z_m}{\sqrt{(x_L - x_m)^2 + (y_L - y_m)^2}}\right) \quad (3.6)$$

Linear relationship between states and the measurements can be obtained by Jacobian matrix. Jacobian matrix of the measurement equations can be written as follows

$$\hat{H} = \begin{bmatrix} \frac{\partial m_1}{\partial x_m} & \frac{\partial m_1}{\partial y_m} & \frac{\partial m_1}{\partial z_m} & \frac{\partial m_1}{\partial v_x} & \frac{\partial m_1}{\partial v_y} & \frac{\partial m_1}{\partial v_z} & \frac{\partial m_1}{\partial b_x} & \frac{\partial m_1}{\partial b_y} & \frac{\partial m_1}{\partial b_z} & \frac{\partial m_1}{\partial x_L} & \frac{\partial m_1}{\partial y_L} & \frac{\partial m_1}{\partial z_L} \\ \frac{\partial m_2}{\partial x_m} & \frac{\partial m_2}{\partial y_m} & \frac{\partial m_2}{\partial z_m} & \frac{\partial m_2}{\partial v_x} & \frac{\partial m_2}{\partial v_y} & \frac{\partial m_2}{\partial v_z} & \frac{\partial m_2}{\partial b_x} & \frac{\partial m_2}{\partial b_y} & \frac{\partial m_2}{\partial b_z} & \frac{\partial m_2}{\partial x_L} & \frac{\partial m_2}{\partial y_L} & \frac{\partial m_2}{\partial z_L} \\ \frac{\partial m_3}{\partial x_m} & \frac{\partial m_3}{\partial y_m} & \frac{\partial m_3}{\partial z_m} & \frac{\partial m_3}{\partial v_x} & \frac{\partial m_3}{\partial v_y} & \frac{\partial m_3}{\partial v_z} & \frac{\partial m_3}{\partial b_x} & \frac{\partial m_3}{\partial b_y} & \frac{\partial m_3}{\partial b_z} & \frac{\partial m_3}{\partial x_L} & \frac{\partial m_3}{\partial y_L} & \frac{\partial m_3}{\partial z_L} \end{bmatrix} \quad (3.7)$$

$$\begin{bmatrix} \frac{x_m - x_p}{r} & \frac{y_m - y_p}{r} & \frac{z_m - z_p}{r} & 0 & 0 & 0 & 0 & 0 & 0 & 0 & 0 & 0 \\ \frac{y_L - y_m}{R_H^2} & \frac{-(x_L - x_m)}{R_H^2} & 0 & 0 & 0 & 0 & 0 & 0 & \frac{-(y_L - y_m)}{R_H^2} & \frac{x_L - x_m}{R_H^2} & 0 & 0 \\ \frac{(z_L - z_m)(x_L - x_m)}{R_H R_T^2} & \frac{-(z_L - z_m)(y_L - y_m)}{R_H R_T^2} & \frac{R_H}{R_T^2} & 0 & 0 & 0 & 0 & 0 & \frac{(z_L - z_m)(x_L - x_m)}{R_H R_T^2} & \frac{(z_L - z_m)(y_L - y_m)}{R_H R_T^2} & \frac{R_H}{R_T^2} & 0 \end{bmatrix} \quad (3.8)$$

where

$$R_H = \sqrt{(x_L - x_m)^2 + (y_L - y_m)^2}$$

$$R_T = \sqrt{(x_L - x_m)^2 + (y_L - y_m)^2 + (z_L - z_m)^2}$$

So that the measurement model can be obtained as

$$\bar{z}_k = \begin{bmatrix} \partial r \\ \partial \lambda_{az} \\ \partial \lambda_{el} \end{bmatrix} = \hat{H} \bar{X}_k + \hat{I}_{3 \times 3} v_k \quad (3.9)$$

where the measurement noise, v_k , is assumed to be uncorrelated, zero-mean, Gaussian noise with covariance matrix \hat{R} as defined Eq. (3.10).

$$v_k \sim N(0, R) \quad , \quad \hat{R} = \text{diag}([\sigma_r^2 \quad \sigma_\lambda^2 \quad \sigma_\lambda^2]) \quad (3.10)$$

3.2 The Tuning and The Initialization of the Filter

The tuning of the Kalman Filter consists of selecting three matrices [8]. These matrices are noise covariance matrix, \hat{Q}_k , measurement noise matrix, \hat{R}_k , and the initial error covariance matrix, \hat{P}_0 . The tuning of the Kalman Filter is highly related to the stability of the filter. The ratio of the error covariance matrix, \hat{P}_k , and measurement noise matrix, \hat{R}_k , is critical due to they are used to calculate Kalman gains, \hat{K}_k . If P/R is too small, filter converges too slowly [8]. On the other hand, if P/R is too large, filter outputs are more affected by the measurement noises. The

effects of P/R on the filter outputs are shown in Figure 3-1. Optimal P/R should be selected, and it is selected by the trial and error in most real applications.

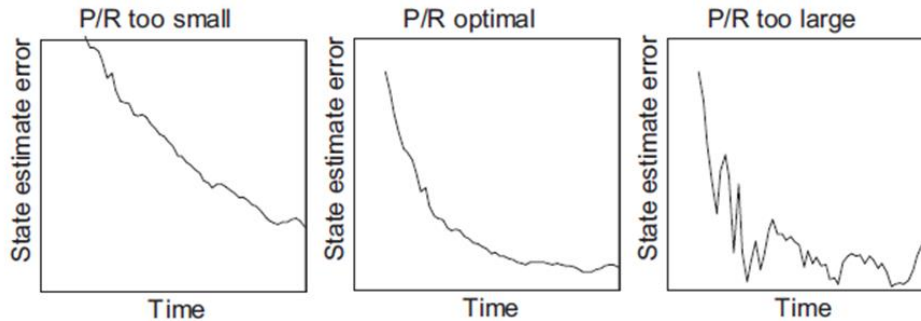


Figure 3-1 Kalman Filter behavior for varying P/R ratio [8]

The process of the filter tuning used in this study is as given below

- Noise covariance matrix, \hat{Q}_k , is constituted by accelerometer data sheet for velocity states. Also, small uncertainty (2 meters) is added to landmark states in \hat{Q}_k to increase the stability of the filter.
- Measurement noise matrix, \hat{R}_k , is constituted by the seeker and datalink datasheets. To be on the safe side, standard deviation of random noise provided by the datasheet is multiplied by 2.
- Since initial covariance matrix must be positive definite [8], the diagonal element of the matrix should be selected non-zero and positive values. There are two approaches to select the initial covariance matrix. The first method is that if the time when the filter starts is known, accumulated INS errors can be estimated and the initial error covariance matrix can be set by this knowledge. Starting time propagation step without waiting for the measurement is also another strategy for initial error covariance matrix.

The initialization of Kalman Filter is another important subject to be taken care of. Since the system is modeled by the error-states, it is a common strategy to start filter with a reset [8]. When the filter outputs the errors, they can be subtracted from the INS solution to get the corrected INS results. In other words, the INS solution can be used to correct itself. On the other hand, the position of the landmark is not known

at the beginning of the filter. So, the only initialization process should be applied to the landmark position.

The first measurement of the seeker can be used to guesstimate the position of the landmark. The process starts when the first measurement of seeker is available, when the seeker locks on the landmark, and is done as follows: landmark's altitude is taken as zero. Using missile's altitude, range between missile and the landmark is calculated, and then using LOS angles, the unit vector pointing the landmark is calculated. Multiplying range and unit LOS vector gives the LOS vector. Finally, it can be added to the missile position to get the landmark position.

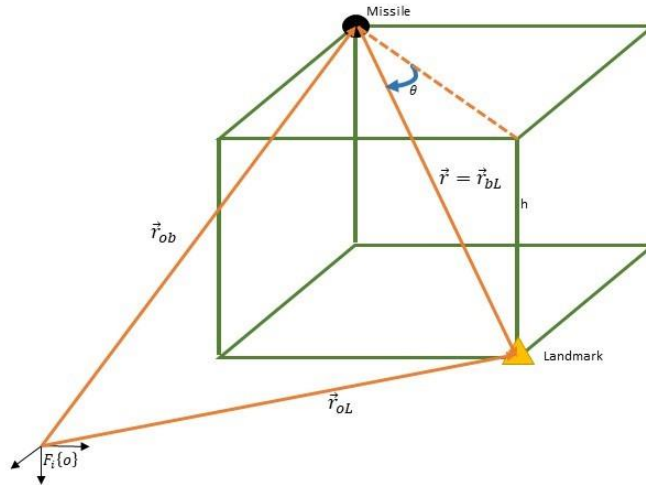


Figure 3-2 Missile and landmark geometry

As can be seen from Figure 3-2 and explained before, LOS vector, \vec{r} , is calculated by geometric relationships. The range can be calculated by geometry as follows

$$|\vec{r}| = r = \frac{h}{\sin(\theta)} \quad (3.11)$$

where h is the altitude of the missile (the altitude of the landmark is assumed to be zero at first), and θ can be calculated by using DCM that gives the rotation matrix from the seeker frame to the inertial frame from Eq. (3.12) [14]

$$\theta = \sin^{-1} \left(\hat{C}^{(i,s)}(3,1) \right) \quad (3.12)$$

The unit LOS vector can be calculated by multiplying rotation matrix from the seeker frame to the inertial frame and the unit vector along the x-axis.

$$\bar{u}_{bL}^{(i)} = \hat{C}^{(i,s)} \begin{bmatrix} 1 \\ 0 \\ 0 \end{bmatrix} \quad (3.13)$$

The initial landmark position is calculated as

$$\bar{r}_{oL}^{(i)} = \bar{r}_{ob}^{(i)} + r \cdot \bar{u}_{bL}^{(i)} \quad (3.14)$$

This calculation is only used at the beginning of the filter. In addition, it can be seen from Eq. (3.14), initializing landmark position is affected by the accumulated INS position error, and seeker gimbal angles which have the uncorrelated, zero-mean, Gaussian noise.

In this chapter, 3-D implementation of the proposed method is explained. In Chapter 4, the mathematical model presented in this chapter is tested by using simulation and experimental methods.

CHAPTER 4

SIMULATIONS AND DISCUSSIONS

In this chapter, the performance of the algorithm described in the previous chapter is studied. In the first part, filter performance is discussed for different accelerometer grades. In the second part, the sensitivity to measurement noise is investigated. Then, sensitivity to the landmark initialization is studied. After that, algorithm is tested, where all errors are included simultaneously. Finally, the algorithm is tested in hardware-in-the-loop (HWIL) environment.

All simulations are run in the 4-DOF simulation environment. The idea of the 4-DOF simulation comes from obtaining the body angular rates in terms of body velocity and acceleration. Body angular rates are calculated by the following kinematics equation

$$\vec{\omega}_B = \frac{\vec{v}_B \times \vec{a}_B}{v_B^2} \quad (4.1)$$

where $\vec{\omega}_B$ is the body angular rates, \vec{v}_B is the body velocity, and \vec{a}_B is the acceleration of the missile produced by the guidance law.

The details of the 4-DOF simulation is given in Appendix B. For the Monte Carlo simulation the missile is skid-to-turn (STT), which means the roll angle is kept at zero. For the HWIL tests, the missile is bank-to-turn (BTT), which means it banks to keep the acceleration on the pitch axis. As explained in Appendix B, the first component of the body angular rates can be used as the designer's desires. For the STT flight, the first component of the angular rate can be obtained by using the following equation [15]

$$\begin{bmatrix} \dot{\phi} \\ \dot{\theta} \\ \dot{\psi} \end{bmatrix} = \begin{bmatrix} 1 & \sin\phi \tan\theta & \cos\phi \tan\theta \\ 0 & \cos\phi & -\sin\phi \\ 0 & \sin\phi \sec\theta & \cos\phi \sec\theta \end{bmatrix} \begin{bmatrix} p \\ q \\ r \end{bmatrix} \quad (4.2)$$

If the first row of Eq. (4.2) is equated to zero, p can be found as

$$p = -(\sin\phi \tan\theta q + \cos\phi \tan\theta r) \quad (4.3)$$

Eq. (4.3) guarantees that missile's initial roll angle will be kept constant, so that choosing initial roll angle as zero, missile flies in STT mode.

4.1 Simulation and HWIL Test Scenario

The missile is released from the platform at 3000 m altitude with 300 m/s initial velocity in the x-axis. After the platform releases the missile, it does U-shape maneuver. The target is located at 15000 m in downrange, and 3000 m in crossrange. The landmark which is locked by the seeker is located at 10000 m in downrange, and 1500 m in crossrange.

The following figures show the missile and the platform nominal trajectories.

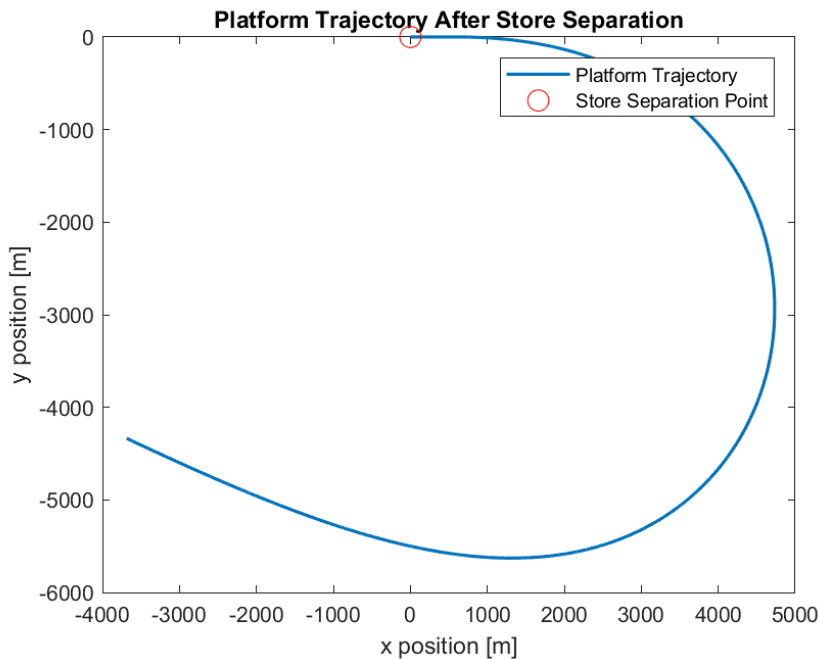


Figure 4-1 Platform trajectory, u-shape maneuver at the constant altitude

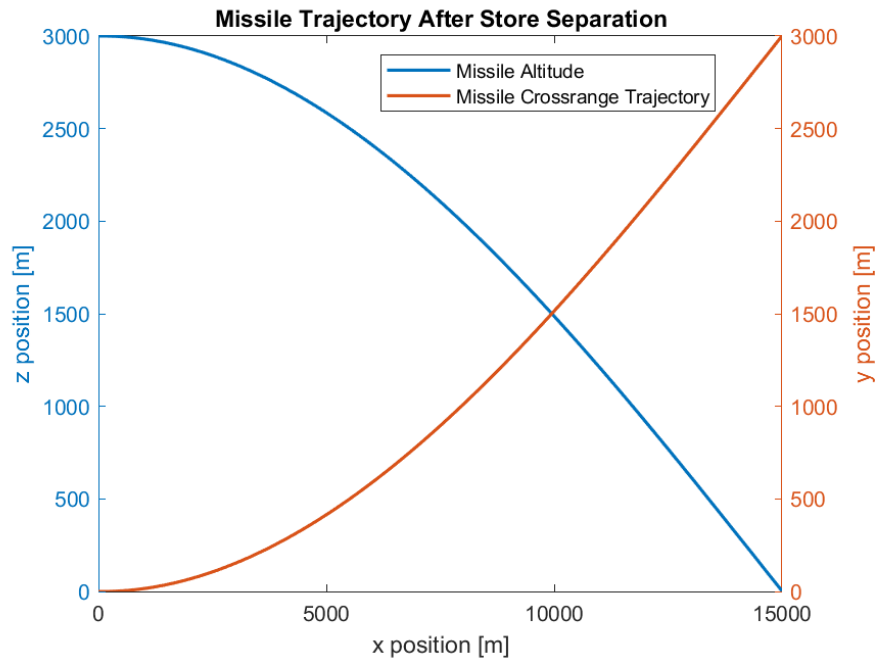


Figure 4-2 Missile trajectories in pitch and yaw planes

In all Monte Carlo simulations and the HWIL tests, the initial INS errors are taken as uniformly distributed errors, and given in Table 4-1. Other errors are given at the relevant section.

Table 4-1 Uniformly distributed initial INS errors for Monte Carlo runs and HWIL tests

Parameters	Errors
Initial Position errors (1σ)	[20;30;10] m
Initial Velocity errors (1σ)	[5;4;2] m/s

The missile approaches to the target by using proportional navigation guidance (PNG), and the navigation gain is selected as 3.

Further assumptions made for the seeker and data link models are listed as follows:

- The gimbal angles are provided by the encoders mounted on the seeker gimbal.

- Limited field of regard (FOR) for inner, and outer gimbal is considered.
- For the Monte Carlo runs, ideal tracking for seeker is assumed, but in HWIL, real passive seeker is used, which has communication and tracking delay.
- For the Monte Carlo runs, unity gimbal dynamics is assumed. However, in HWIL, real seeker is used, which does not have unity gimbal dynamics.
- Datalink signal is never lost.

4.2 Sensitivity to Errors

4.2.1 Sensitivity to Acceleration Errors

In this section, filter performances for two different accelerometers are compared. The first accelerometer is selected as tactical-grade. The second accelerometer is selected as consumer-grade. The only errors for the accelerometers are constant bias error and an uncorrelated, zero mean additive Gaussian noise. The error values are selected as an average value of the relevant grade [8]. The errors that will be considered are given in Table 4-2.

Table 4-2 Accelerometer sensor specifications

Parameter	Tactical-grade	Consumer-grade
Bias	0.01 m/s ²	0.3 m/s ²
Random-noise (1σ)	0.002 m/s ²	0.06 m/s ²

Each simulation consists of 500 runs with randomly generated accelerometer errors. Since, in this part, accelerometer errors' effects are investigated, seeker and datalink measurement errors are kept constant and relatively small value. Chosen values are given in Table 4-3. Also, measurement is updated with 10 Hz frequency.

Table 4-3 Datalink and seeker measurement errors used for testing sensitivity to accelerometer errors

Parameter	Data link	Seeker
Random-noise (1σ)	0.1 m	0.001 deg

Figure 4-3, Figure 4-4, and Figure 4-5 show missile position, velocity, and landmark position errors in the case where tactical-grade accelerometer is used. As expected, INS errors are well compensated by the algorithm. Because of the seeker gimbal limits, lock is lost around 25 sec, and it is shown in the figures by vertical dashed line. In the figures, solid lines are the arithmetic average of the corresponding data, and dashed line shows their $\pm 1\sigma$ band.

When the seeker reaches its gimbal limits and the filter stops, last estimated accelerometer bias is held. So that after the filter stops, the accumulation rate of errors is reduced. Vertical dashed line indicates the time when the EKF stops.

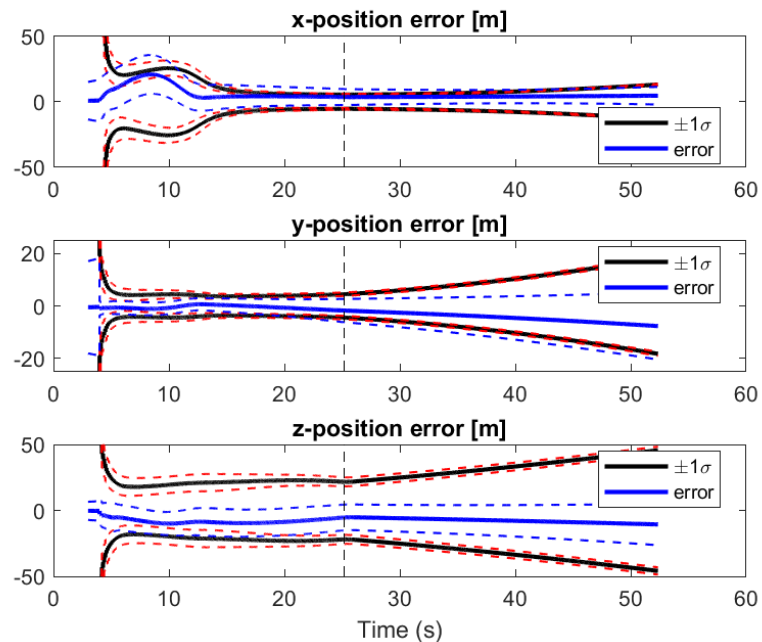


Figure 4-3 Missile position error for tactical-grade case

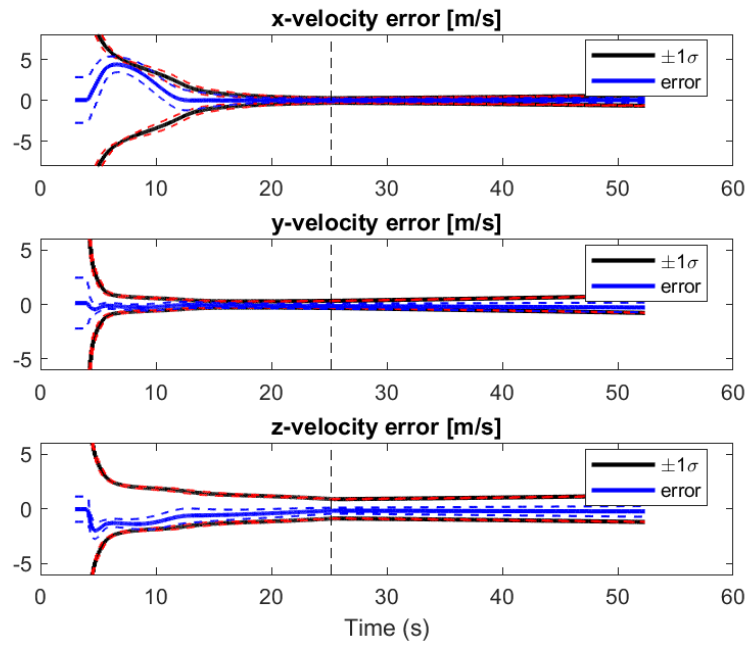


Figure 4-4 Missile velocity error for tactical-grade case

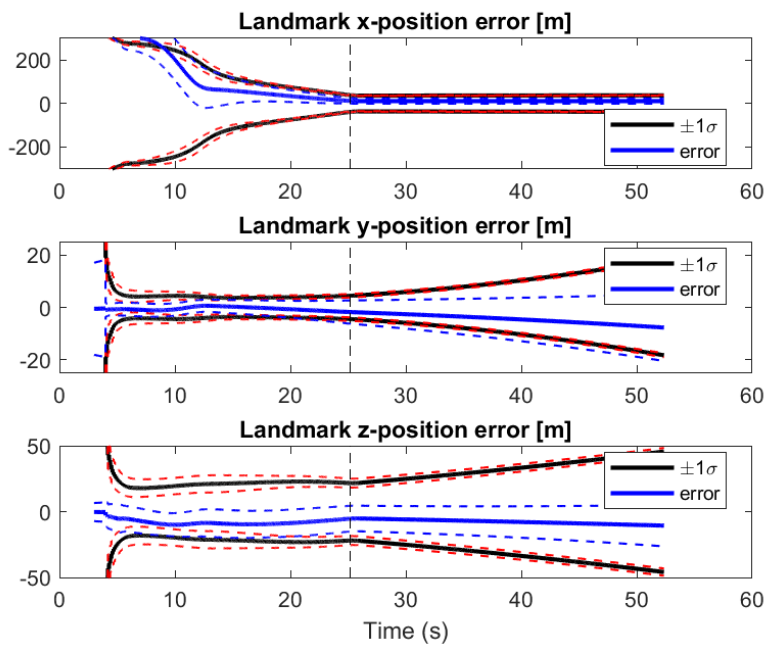


Figure 4-5 Landmark position error for tactical-grade case

Zoom view of Figure 4-4 is also shown below

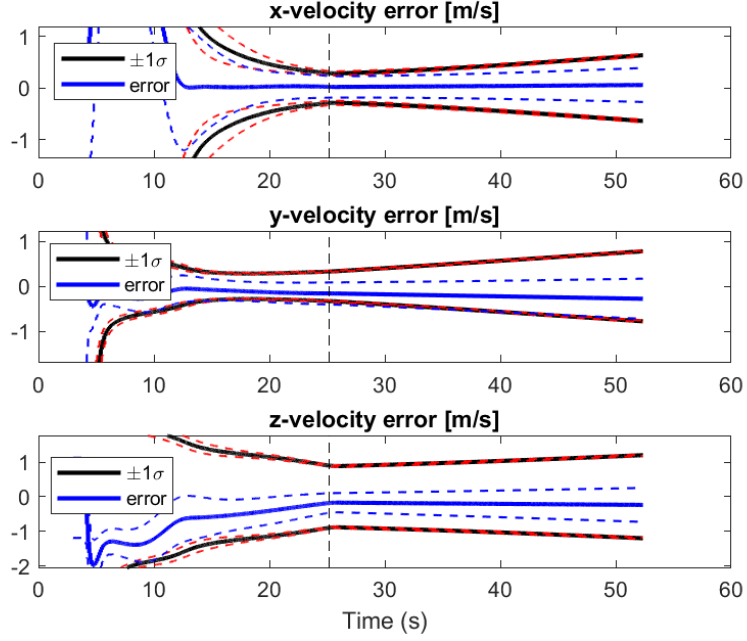


Figure 4-6 Zoom view of Figure 4-4

The root-mean-square error (RMSE) is used to provide more insight into the performance of the algorithm. The proposed algorithm is compared to INS-only results. RMSE is calculated as follows [8]

$$RMSE_k = \sqrt{\frac{1}{n_{mc} - 1} \sum_{n=1}^{n_{mc}} (\bar{x}_k - \bar{x}'_k)^2} \quad (4.4)$$

where n_{mc} is the total number of the Monte Carlo runs. \bar{x}_k is the estimation of the filter, and \bar{x}'_k is the true value at the time k .

The RMSE results for tactical-grade accelerometer are given in Figure 4-7, Figure 4-8, Figure 4-9. Figure 4-7 shows the RMSE of the position. As expected, the INS-only results accumulate with time, whereas the EKF results compensate errors with time. The filter does not estimate biases perfectly since actual bias values are quite

small. In real applications, estimated tactical-grade biases usually are not used in feedback for GPS-INS integration because of being small.

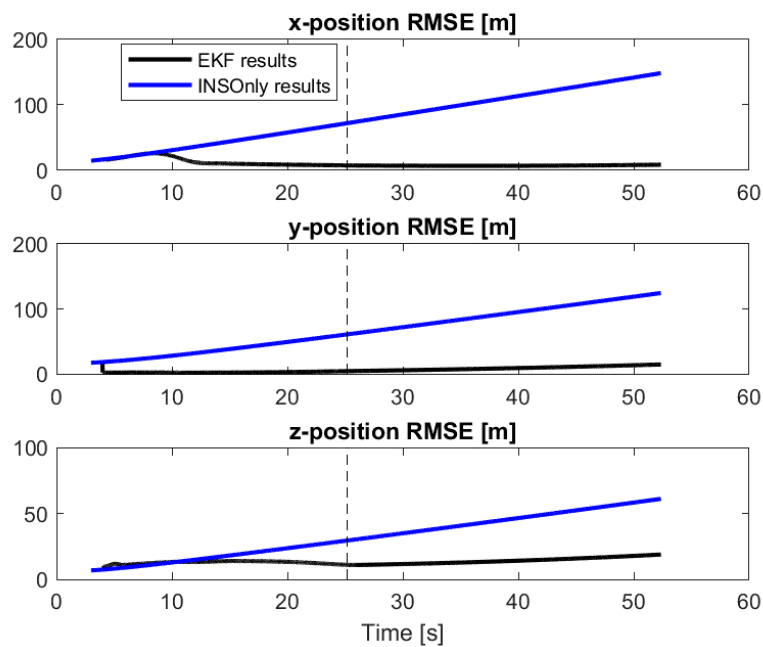


Figure 4-7 RMSEs of position errors for EKF results and INS-only results (tactical-grade, 500 runs)

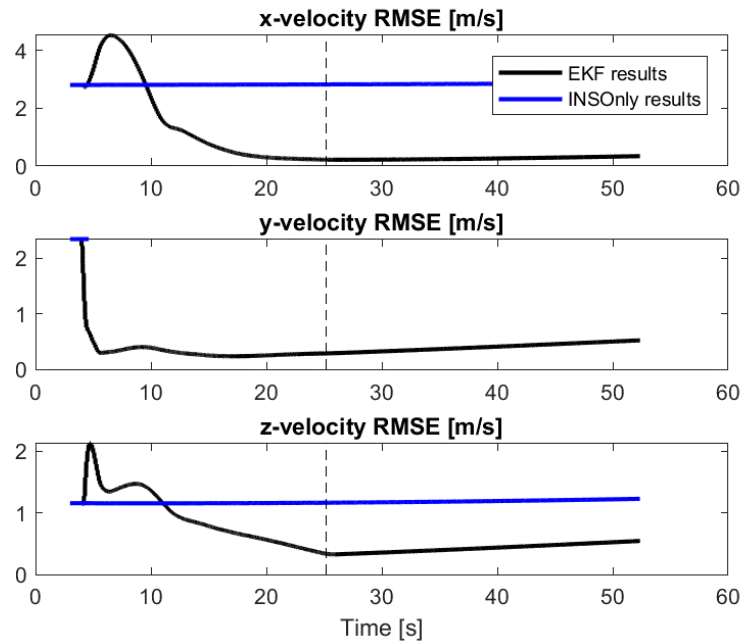


Figure 4-8 RMSEs of velocity errors for EKF results and INS-only results (tactical-grade, 500 runs)

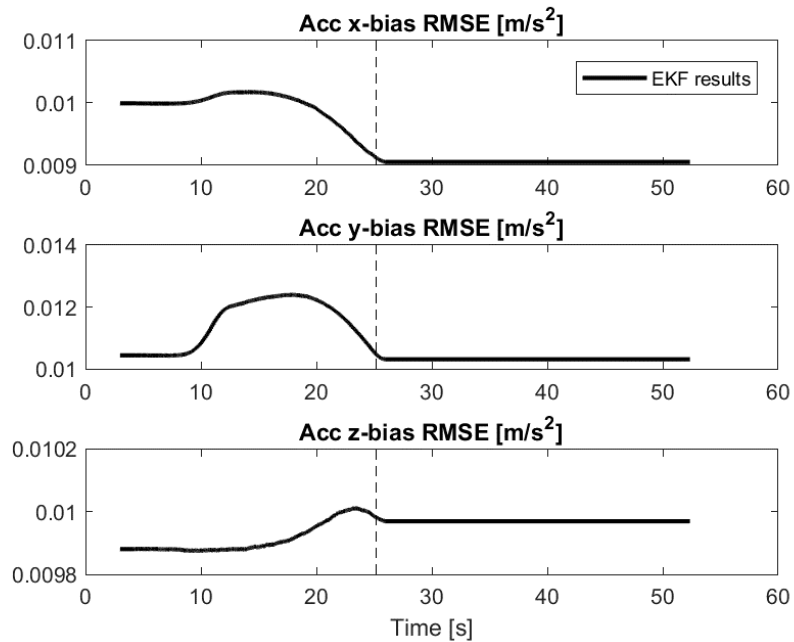


Figure 4-9 RMSEs of the accelerometer bias errors (tactical-grade, 500 runs)

The INS-only results accumulate with time and diverge, as it can be seen from Figure 4-7. Figure 4-10 shows the close view of the Figure 4-7, where the EKF results show superior performance. The INS-only results accumulate error more than 100 m in x and y-axis, and more than 50 m in z-axis. On the other hand, the EKF decreases the error to the less than 10 m in x and y-axis, and less than 20 m in z-axis.

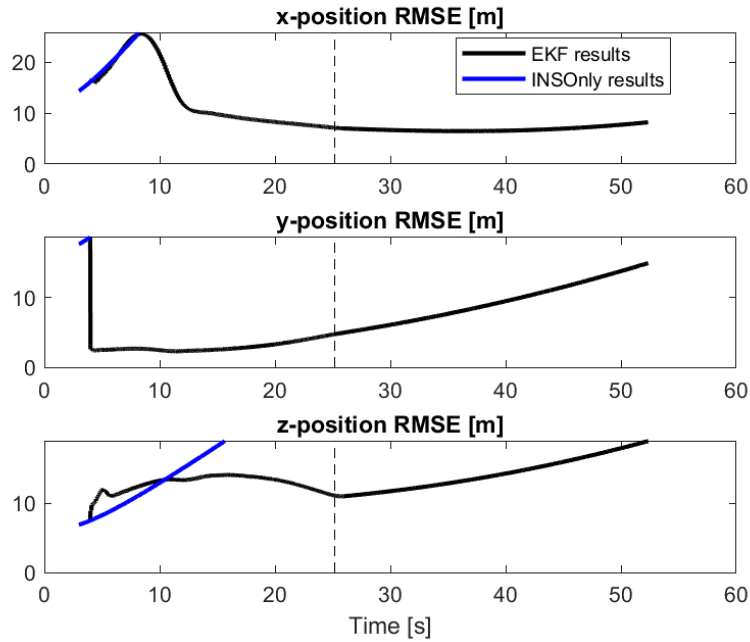


Figure 4-10 Zoomed view of Figure 4-7

RMSE results for consumer-grade accelerometer are given in Figure 4-11, Figure 4-12, Figure 4-13. Figure 4-11 shows the RMSE of the position. Same with the tactical-grade accelerometer, the INS-only results accumulate with time, whereas EKF results compensate errors with time. The compensation is more drastic in this scenario since accelerometer biases and noises of consumer-grade are higher than tactical-grade. From Figure 4-13, it can be concluded that the filter can estimate biases better than it did in the tactical-grade case. The reason is that the bias terms of the consumer-grade accelerometer are high-valued enough to be compensated whereas the bias terms of the tactical-grade accelerometer are low-valued, so that, they can not be compensated.

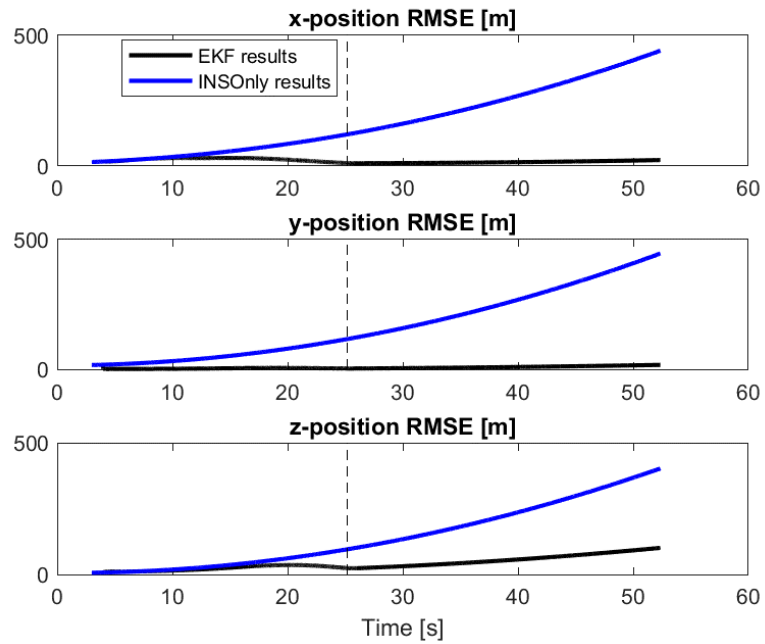


Figure 4-11 RMSEs of position errors for EKF results and INS-only results (consumer-grade, 500 runs)

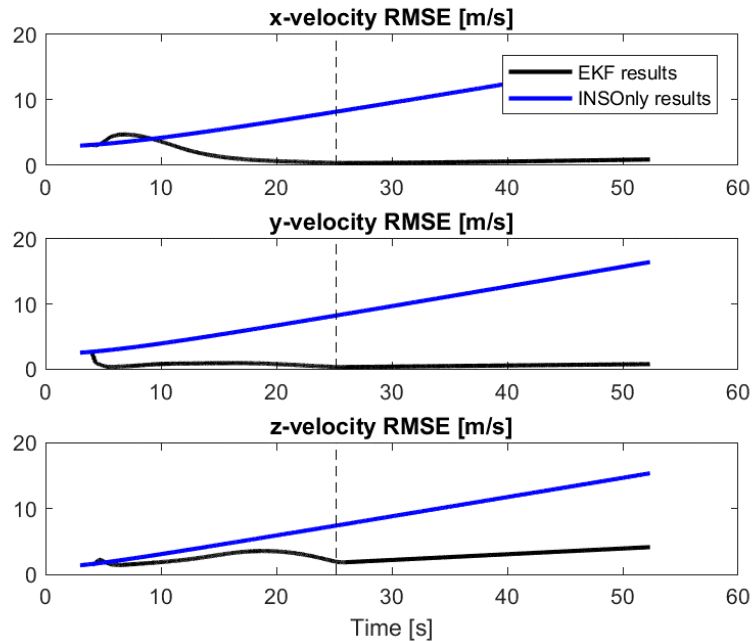


Figure 4-12 RMSEs of velocity errors for EKF results and INS-only results (consumer -grade, 500 runs)

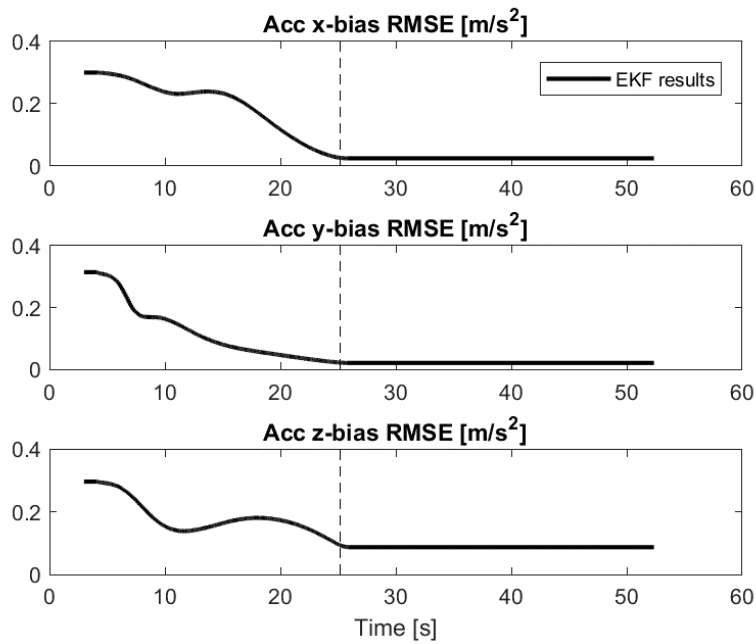


Figure 4-13 RMSEs of the accelerometer bias errors (consumer-grade, 500 runs)

Close view of the Figure 4-12 and Figure 4-13 are shown below. If the proposed EKF is not used, the errors of the INS-only solution accumulate more than 400 m in 50 s. On the other hand, the proposed method can reduce the errors less than 20 m in x- and y-axis, and less than 100 m in z-axis.

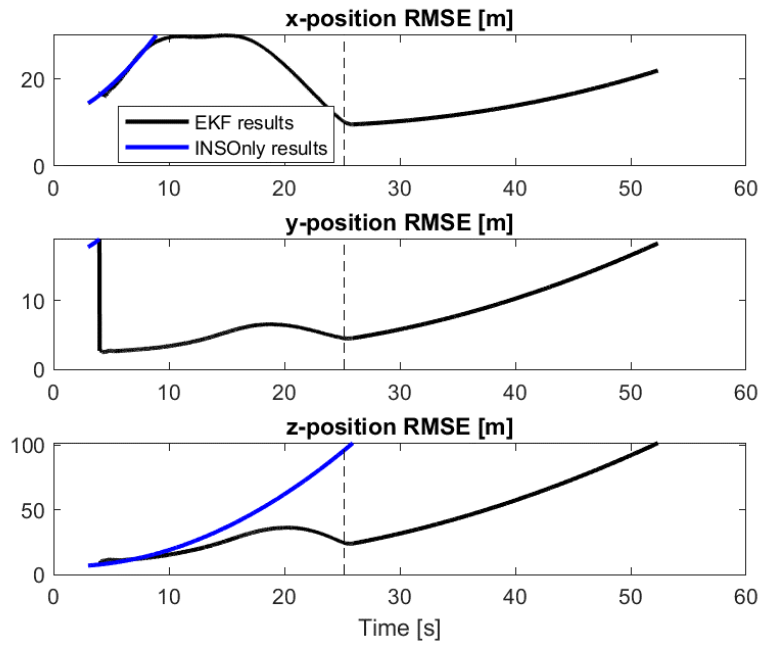


Figure 4-14 Zoomed view of Figure 4-12

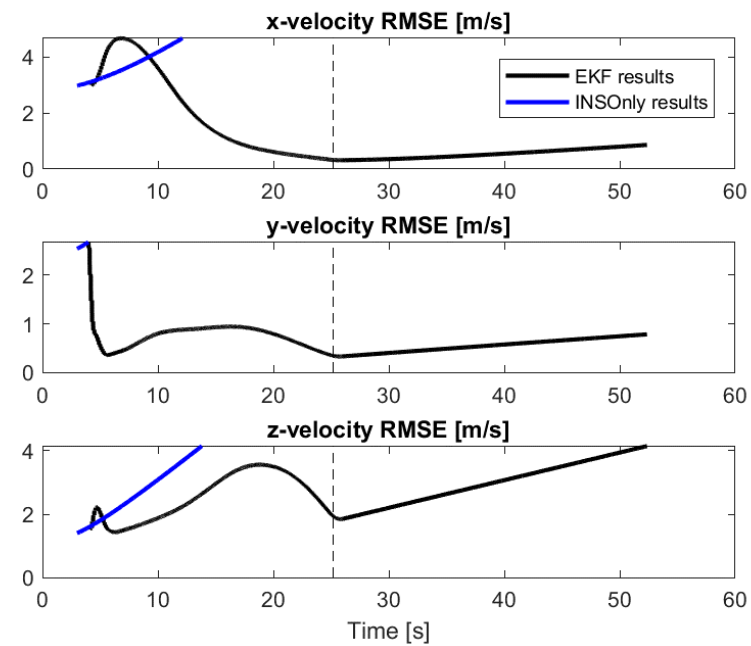


Figure 4-15 Zoomed view of Figure 4-13

4.2.2 Sensitivity to Data Link and Seeker Measurement Errors

As explained before, the data link and the seeker are essential for the proposed algorithm. Their measurements are integrated with the inertial measurements to obtain a better navigation solution. In this section, the performance of the algorithm is investigated in terms of data link range and seeker gimbal angle measurements. The algorithm is tested for different measurement error levels. The standard deviation of the data link range measurement is selected from [8] for different grades. The standard deviation of the seeker measurements is defined by the resolution, which is the minimum difference encoder can read, how many steps in a single revolution. For instance, 16-bit encoder's resolution is $360/2^{16} = 0.0055$ [deg]. Selected error levels are given in Table 4-4.

Table 4-4 Datalink and seeker measurement errors for testing algorithm sensitivity to datalink and seeker measurement errors

	Data link random noise (1σ)	Seeker random noise (1σ)
Case1	1 [m]	0.01 [deg]
Case2	1 [m]	0.1 [deg]
Case3	10 [m]	0.01 [deg]
Case4	10 [m]	0.1 [deg]

Figure 4-16, Figure 4-17 show the RMSE of the position and velocity for the cases given above. The worst results belong to case4, which has the highest random noises. From Figure 4-16, Figure 4-17, It can be said that altitude position and velocity results are better for case1 and case3, which indicates altitude position and velocity results are highly dependent to seeker random noise level.

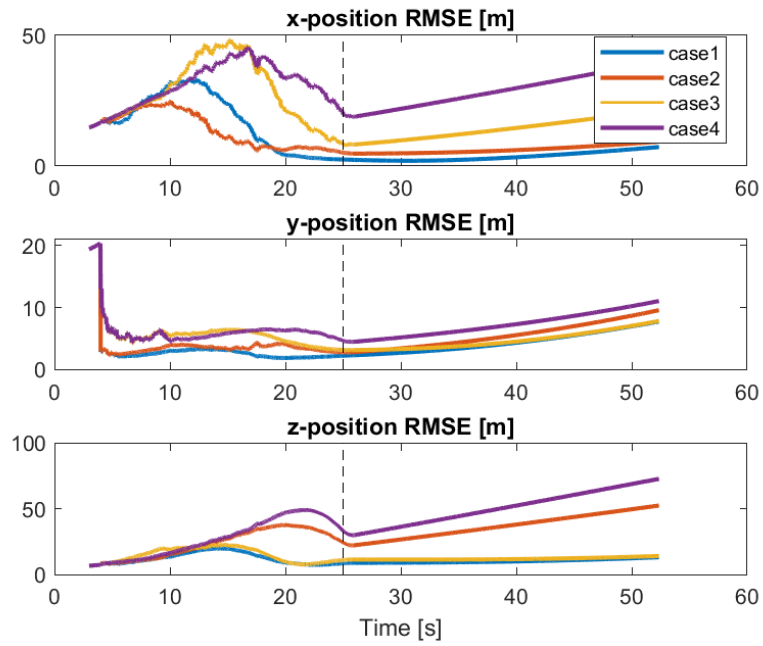


Figure 4-16 RMSE of position for different cases

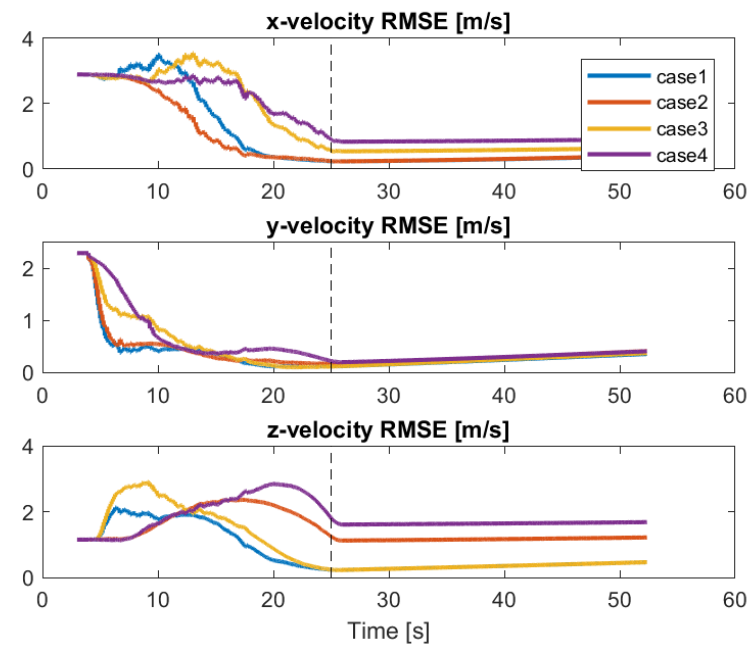


Figure 4-17 RMSE of velocity for different cases

4.2.3 Sensitivity to Landmark Initialization

Initial landmark errors depend on the accumulated INS errors and seeker measurement errors, and actual altitude of the landmark as it can be seen from Eq. (3.14). In this part, algorithm is tested in terms of landmark initial errors. Since only the effect of the landmark initial errors is aimed to be tested, other errors are kept small. All error levels are given in Table 4-5.

Table 4-5 Datalink, seeker, and accelerometer errors and different landmark altitudes to test algorithm sensitivity to landmark initial error

	Landmark's real altitude	Data link random noise (1σ)	Seeker random noise (1σ)	Accelerometer grade
Case1	0 [m]	1 [m]	0.01 deg [deg]	Tactical
Case2	100 [m]	1 [m]	0.01 deg [deg]	Tactical
Case3	500 [m]	1 [m]	0.01 deg [deg]	Tactical
Case4	1000 [m]	1 [m]	0.01 deg [deg]	Tactical

To cover all cases, the elements of the initial covariance matrix, which are related to the landmark position states are selected with respect to the worst case. The last three of the diagonal elements of the covariance matrix are [6000,6000,2000].

Figure 4-18, Figure 4-19 show the RMSE of the position and the velocity of the missile. Eventhough the beginning of the filter results slightly changes, the proposed method can reduce the INS errors for all cases.

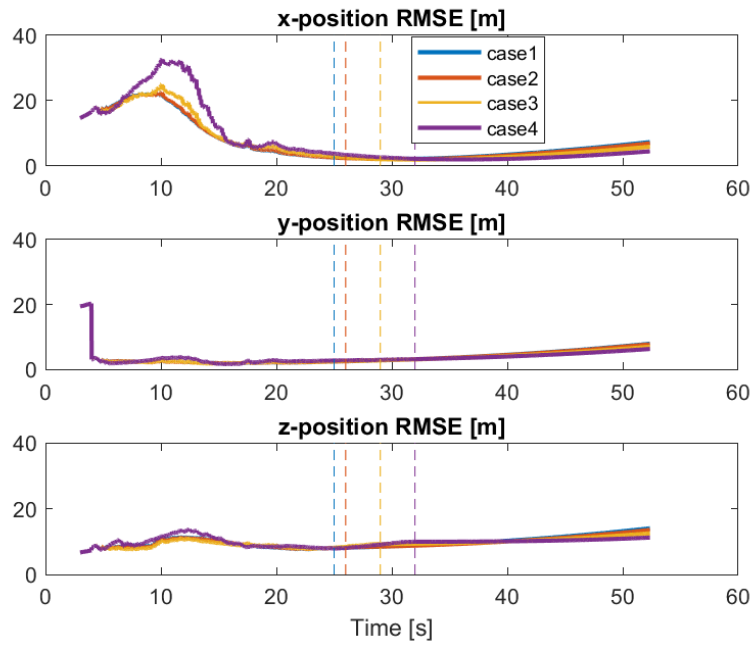


Figure 4-18 RMSE of the missile position in terms of different landmark initial errors

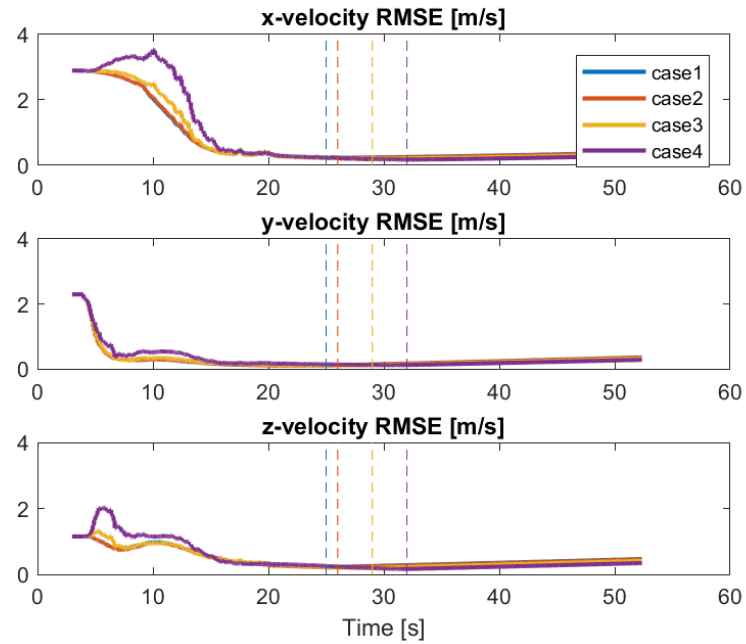


Figure 4-19 RMSE of the missile velocity in terms of different landmark initial errors

4.2.4 Realistic Monte Carlo Results

Finally, all errors can be included to test the algorithm for the more realistic case. For this case, the accelerometer is selected as customer level in which details are given in Table 4-2. The data link error is selected as 1 m for 1σ , and the seeker error is selected as 0.0055° for 1σ , which is the resolution for the 16-bit encoder. The landmark initialization error is selected as 300m.

Figure 4-20, Figure 4-21, Figure 4-22 show the RMSE of the position and the velocity estimation of the missile, with their INS-only counterparts, and the bias estimation of the accelerometer. The results illustrate that the proposed method can compensate INS errors well.

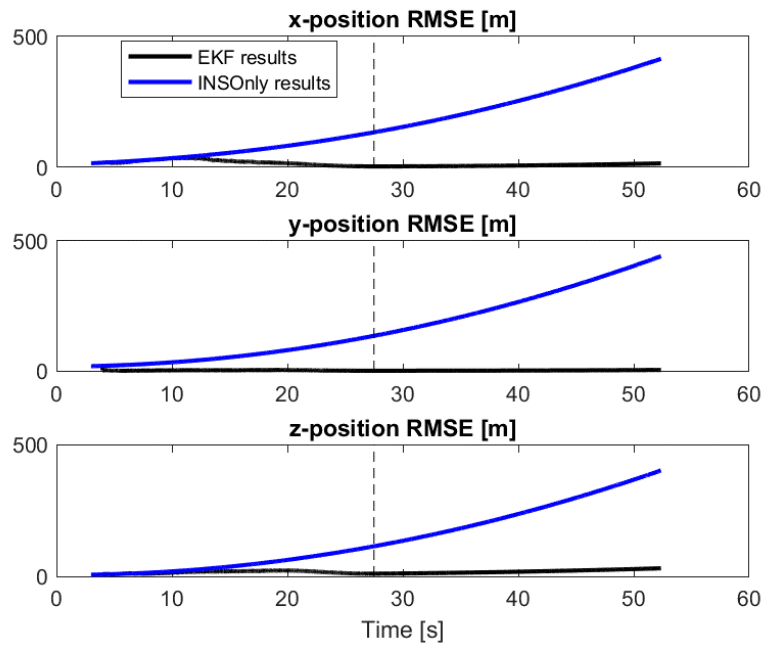


Figure 4-20 RMSE of the missile position when all errors are at a realistic level

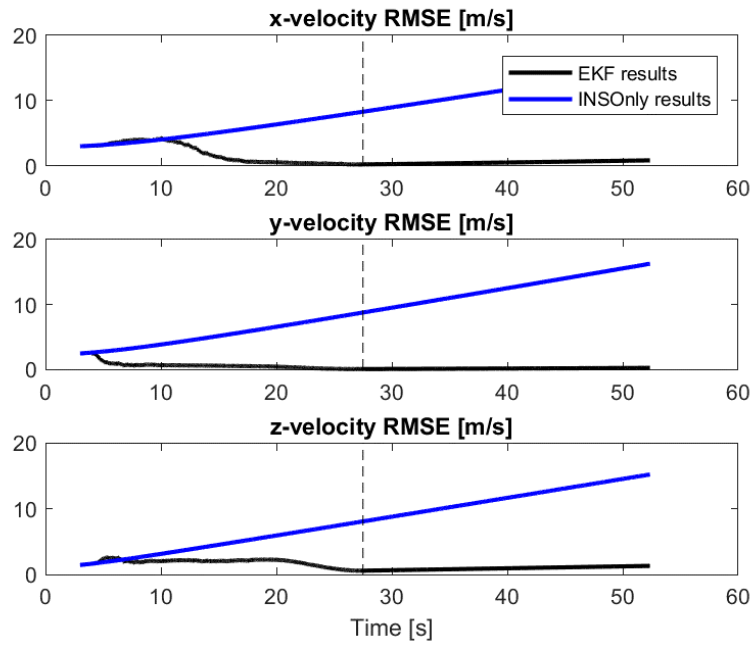


Figure 4-21 RMSE of the missile velocity when all errors are at a realistic level

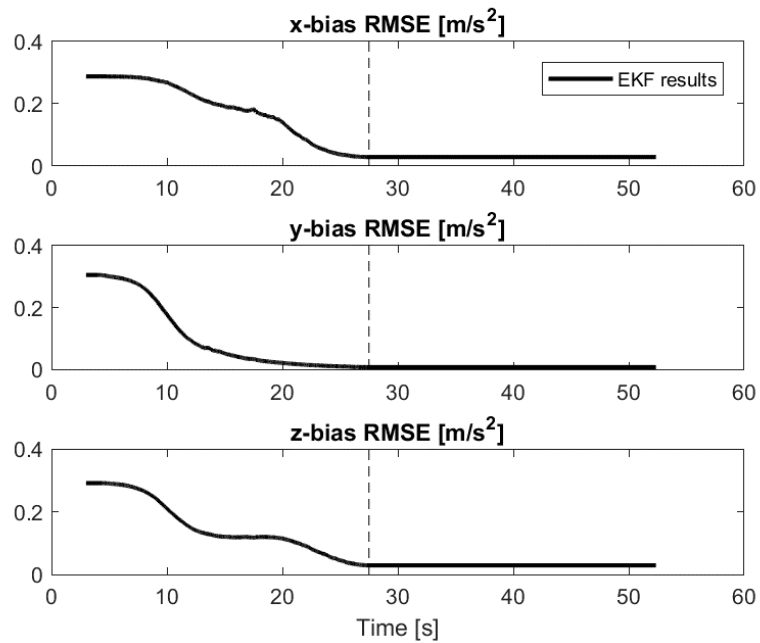


Figure 4-22 RMSE of the bias when all errors are at a realistic level

Close views of Figure 4-20 and Figure 4-21 are shown in the following figures. The figures show that the proposed method can drop the error accumulation of the INS-only solution.

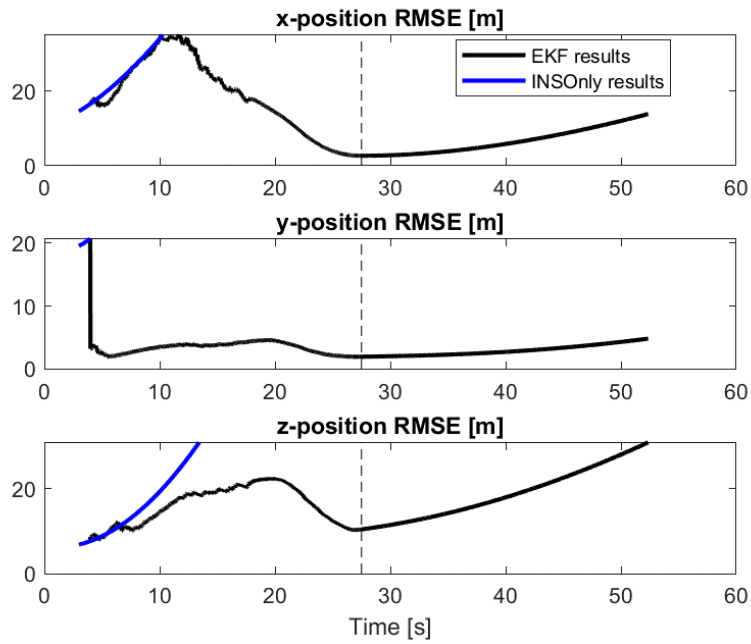


Figure 4-23 Zoomed view of Figure 4-20

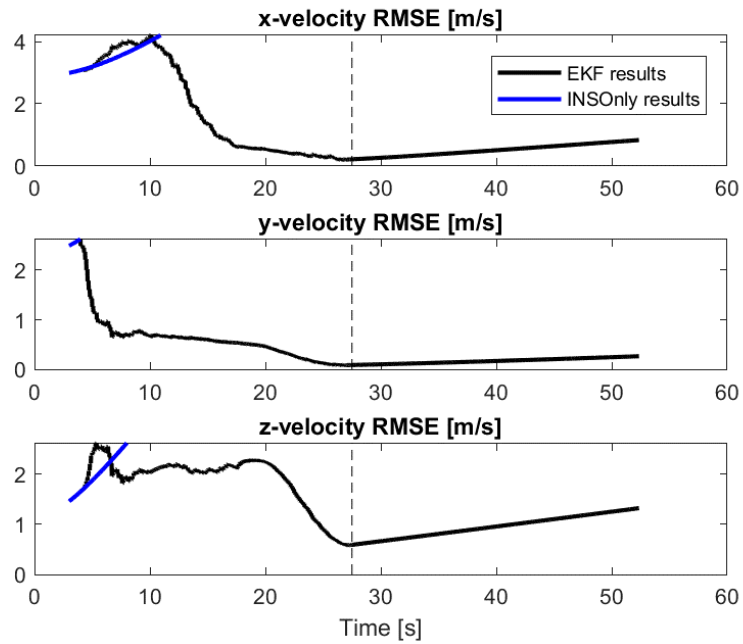


Figure 4-24 Zoomed view of Figure 4-21

4.3 Hardware-In-The-Loop Test Results

The proposed algorithm is tested by a hardware-in-the-loop (HWIL) testbed. The testbed consists of two main parts: the flight-motion-simulator (FMS) and the target-motion-simulator (TMS). Two examples of the FMS-TMS testbed are shown in Figure 4-25 and Figure 4-26. In Figure 4-25, a 3-axis FMS testbed is shown. In Figure 4-26, a 5-axis FMS-TMS testbed is shown.



Figure 4-25 3-axis FMS system [24]

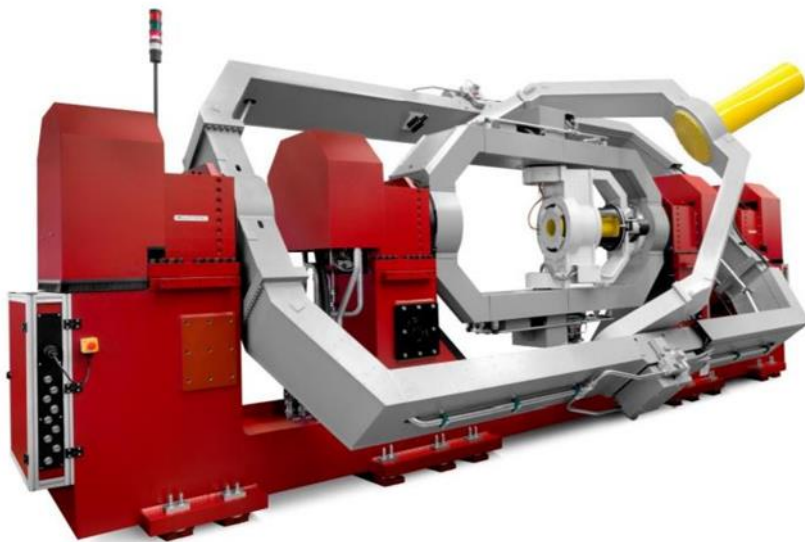


Figure 4-26 5-axis FMS-TMS system [25]

In this study, a 5-axis FMS-TMS testbed is used. The seeker is mounted to the FMS part of the testbed, and the TMS images the scene of the seeker. The data link and the accelerometer measurements are generated by the simulation. The errors are given in Table 4-6. The seeker used in the simulation has a 16-bit resolution.

Table 4-6 Measurement errors of HWIL testbed

Parameter	Accelerometer	Seeker	Data link
Bias	0.01 m/s ²	-	-
Random-noise (1 σ)	0.002 m/s ²	360/2 ¹⁶ deg	1 m

Missile is flired in BTT mode in HWIL tests. The acceleration on y-z plane of the body frame can be seen from Figure 4-27. The purpose is to rotate the body around x-axis so that all acceleration command coincides with the z-axis of the body frame. For this purpose, the roll rate command is calculated by using the proportional control method.

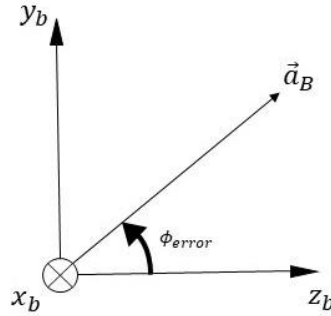


Figure 4-27 Acceleration command on body frame's y-z plane

Roll rate command is calculated by multiplying the roll error with a constant, k.

$$p = k\phi_{error} \quad (4.5)$$

ϕ_{error} can be calculated by the following equation [28], [29].

$$\phi_{error} = \text{atan} \left(\frac{a_{ycom}}{-a_{zcom}} \right) \quad (4.6)$$

where a_{ycom} and a_{zcom} are the second and the third components of the acceleration command in the body frame, respectively.

Applied to the scenario presented in Section 4.1, the performance of the BTT logic is illustrated. Figure 4-28 shows the performance as a function of the control gain, k. The commanded roll rate is limited between ± 20 deg/s for practical concerns. The

performance improves with increasing control gain. $k=2$ is used in the HWIL test, which provides an intermediate performance.

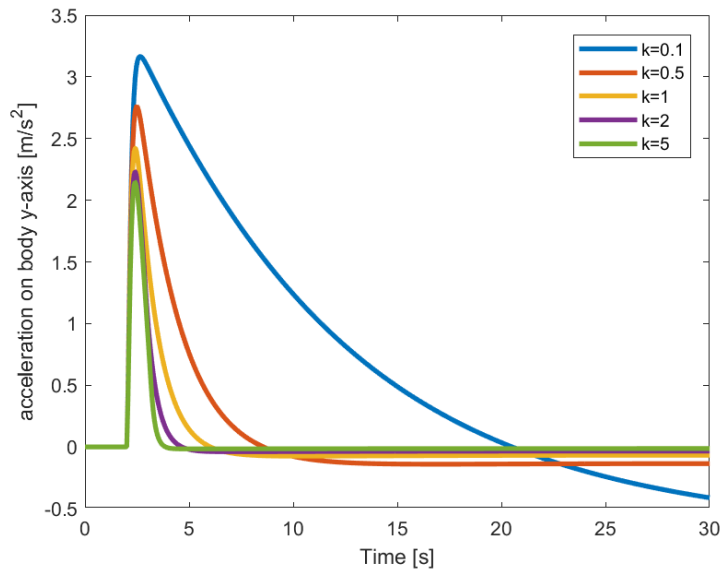


Figure 4-28 Effect of the control gain, k , on the BTT performance

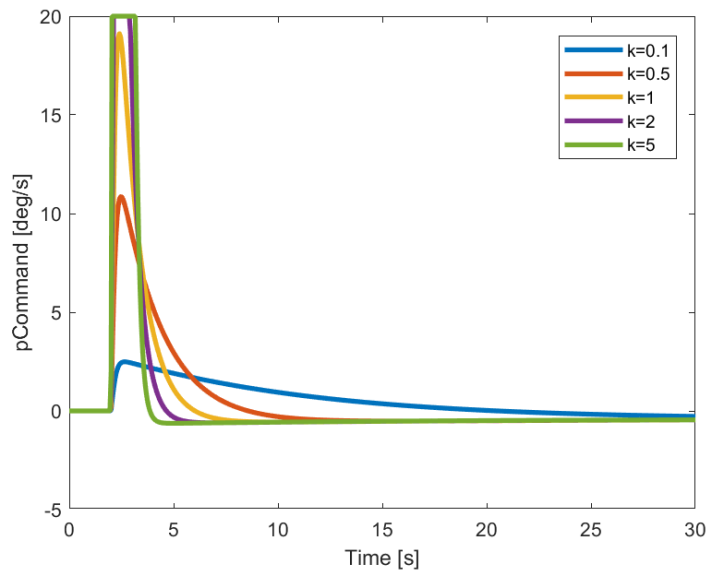


Figure 4-29 Calculated roll rates for different k values

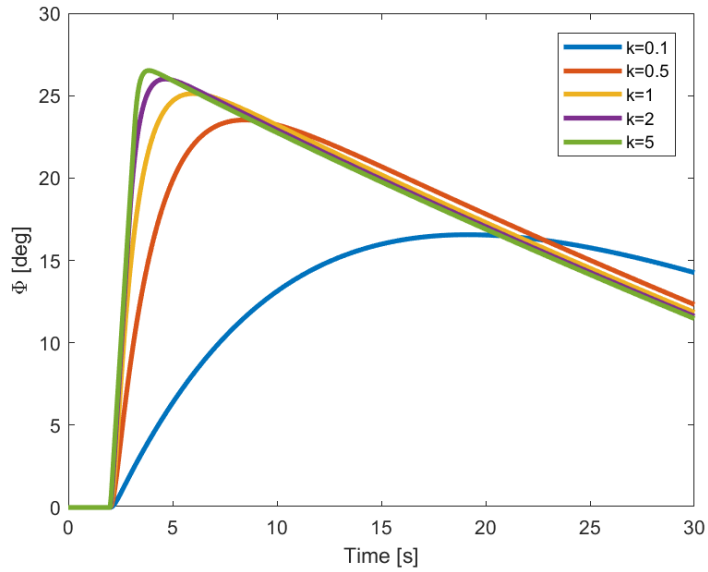


Figure 4-30 Effect of the control gain, k , on the roll angle

Figure 4-31 shows the BTT-model used in 4-DOF simulation.

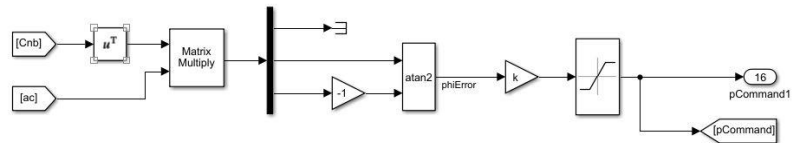


Figure 4-31 BTT logic (Eq. (4.5))

To show the performance of the proposed method, three scenarios are conducted. In the first scenario, the guidance loop is completed by the ideal position, and velocity, where there is no error. In the second scenario, the guidance loop is completed by the INS-only position and velocity results, where errors accumulate in time. In the last scenario, the loop is completed by the position and the velocity of the EKF results. In the last two scenarios, the seeker is used at the terminal phase, in which the seeker manually locks on the target.

Figure 4-32 shows the ideal case. The cursor is always on the target. Figure 4-33 shows the second case where cursor moves away from the target because of the accumulation of the INS errors. Before the target getting out of the scene, seeker is manually locked on the target. In Figure 4-34, the last case is shown. At the beginning stage, seeker is locked on the landmark while moving towards to the target position. When the gimbals reached the limits, seeker pointed to the target. As seen from the second scene of the Figure 4-34, the cursor is not on the target exactly, but

closer than the INS-only case. At the terminal phase, the seeker manually locks on the target.

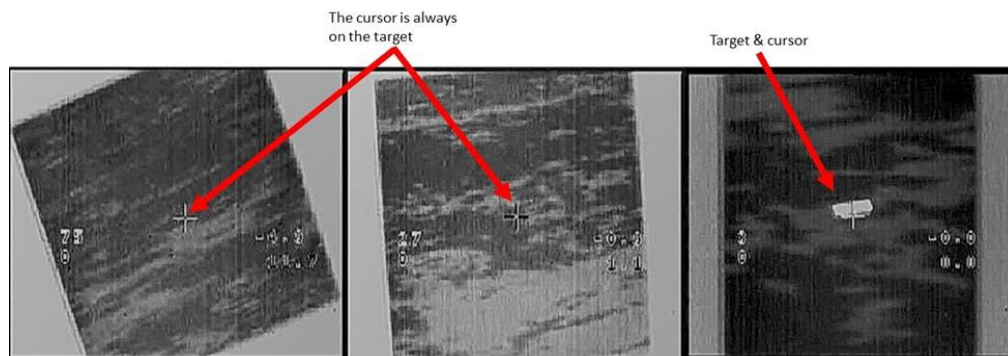


Figure 4-32 Ideal case seeker scenes

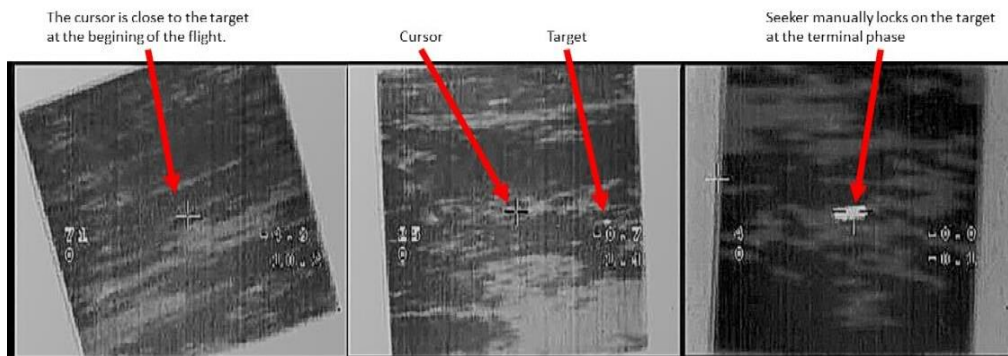


Figure 4-33 INS-only case seeker scenes

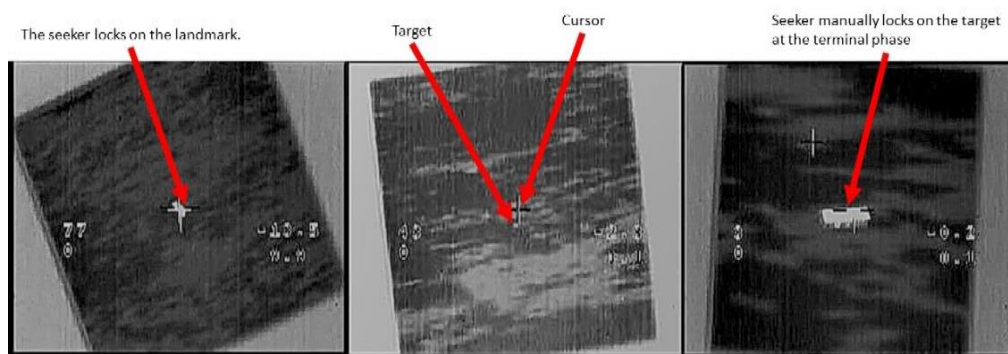


Figure 4-34 INS aided case seeker scenes

Figure 4-35 and Figure 4-36 show the performance of the EKF. As expected INS errors are well estimated and compensated.

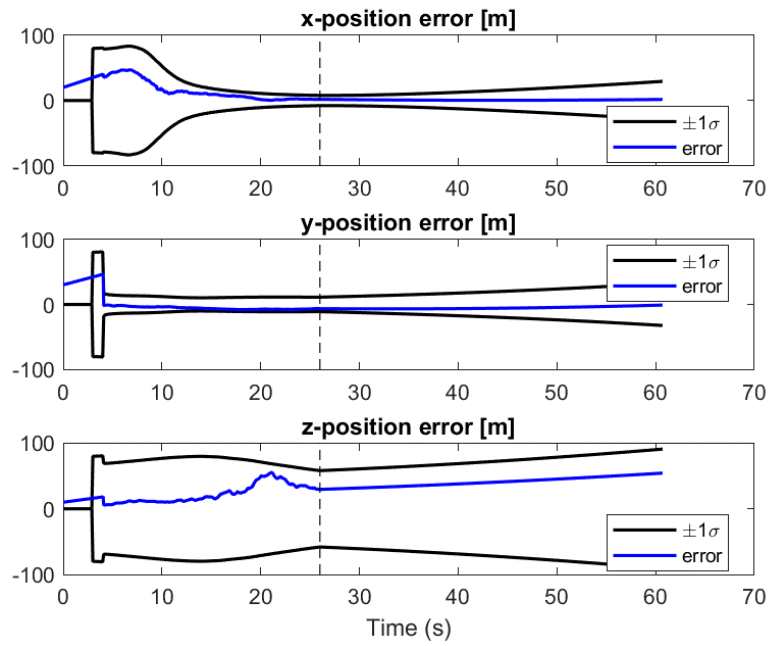


Figure 4-35 Missile position errors

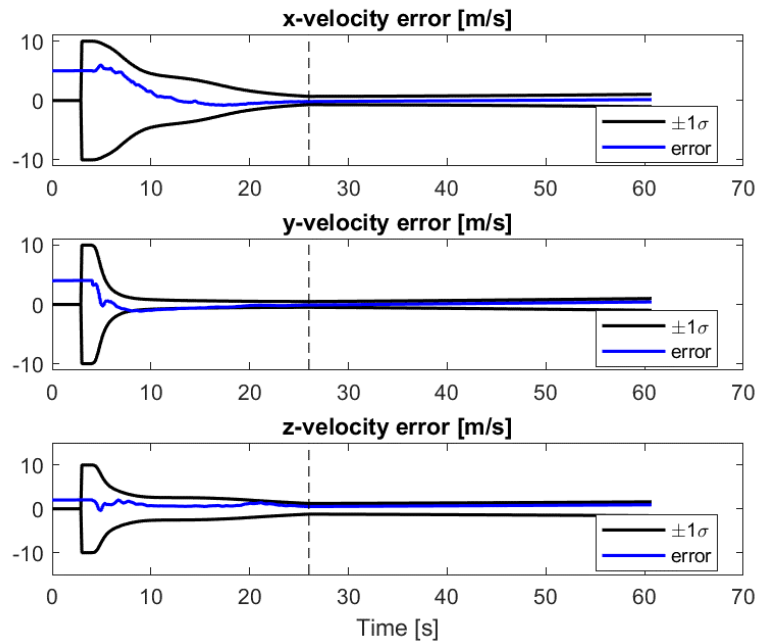


Figure 4-36 Missile velocity errors

Figure 4-37 and Figure 4-38 show the comparison of the INS-only errors and the EKF errors. As it can be seen from Figure 8, the position errors of the INS-only accumulate more than 200 meters in x- and y- axis, and more than 100 meters in z- axis. On the other hand, EKF position errors are less than 1 meter in x- and y- axis, and less than 60 meters in z- axis.

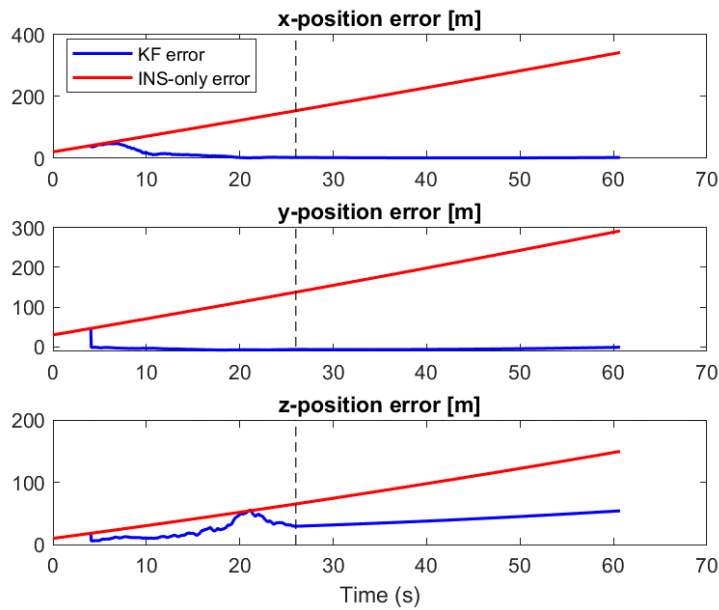


Figure 4-37 Comparison of INS-only and EKF position errors

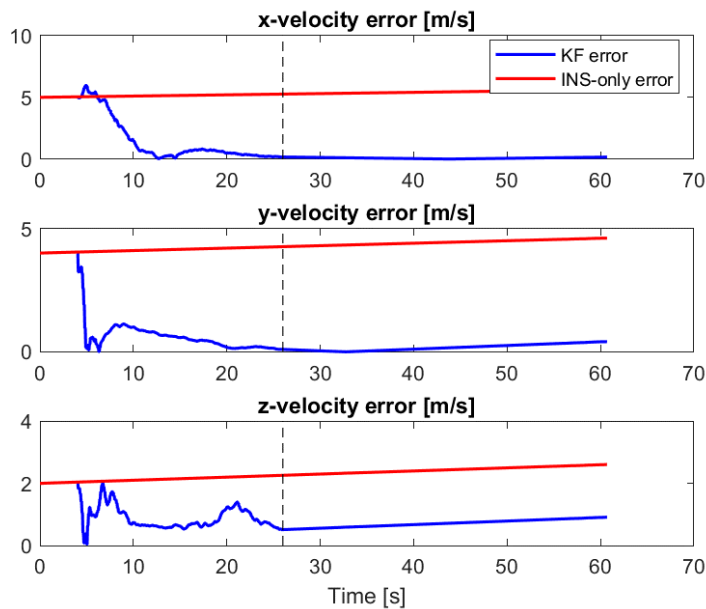


Figure 4-38 Comparison of INS-only and EKF velocity error

CHAPTER 5

CONCLUSION

In this thesis, a novel way of compensating INS errors is investigated. The estimation is performed by utilizing measurements obtained from a data link, a seeker, and a set of accelerometers. The EKF framework is used for this estimation.

The study is composed of two main parts. The first part focuses on the proof of the concept in the plane. For this purpose, external measurements: the range from the data link and the LOS angle from the seeker are implemented in 2D-planar engagement geometry. Three candidate solutions are proposed. The first candidate, which involves only the data link measurement, is identical with the one-satellite GNSS-INS integration, which is well known to be insufficient for improving the INS solution. The second candidate was already studied in the literature where the seeker measurements are integrated with the inertial measurements to increase navigation quality. This method requires the knowledge of the position of the landmark, which is a significant restriction for real applications. After that, the third candidate (the proposed method), which combines two measurements, is implemented. The proposed method does not require the knowledge of the position of the landmark. The simulation results show the proposed method has better performance than the one in the literature and does not require the position of the landmark. The observability of the proposed method is investigated in terms of deterministic and stochastic observability techniques. In addition, by making an analogy, the problem is likened to the target motion analysis problem, which suggests that a non-zero LOS rate is sufficient for the observability of the filter.

The second part of the study is the 3D implementation of the proposed method. The system and the measurement models are extended to 3D. The filter's initialization and tuning are also investigated in that part. The proposed method is tested in Monte

Carlo simulations and the hardware-in-the-loop testbed after the system and the measurement models are obtained. The simulations are conducted in 4-DOF simulation, which provides a constrained 6-DOF simulation environment. All the simulation and the test results show the proposed method can be used as an INS aiding algorithm.

The present study can be improved with the following works:

- Gyroscope errors can be taken into consideration by having six more states: three attitude errors of the missile body and three gyroscope biases.
- In this study, the data link is assumed to be never lost. Loss of data link can be implemented and analyzed.
- In real applications, data link causes a communication delay. The delay can be modeled and implemented into the system.
- Gimballed seekers have also mounted gyroscope, which provides line-of-sight (LOS) angular rate. LOS rate can be included in the system and analyzed.
- The other inertial measurement errors can be considered other than bias, such as scale-factor and misalignment.

To sum up, a novel method for INS error compensation is developed within the scope of addressed errors in this work. Simulation results and the HWIL tests show that the proposed method is successful in each case.

REFERENCES

- [1] I. Y. Bar-Itzhack, "Optimal Updating of INS Using Landmarks.," Tech. Isr Inst Technol TAE Rep, no. 301, 1977.
- [2] H. Rotstein, J. Reiner, and A. Ben-Ishai, "Kalman Filter Mechanization in INS/Seeker Fusion and Observability Analysis," in AIAA Guidance, Navigation, and Control Conference and Exhibit, 2001.
- [3] W. Hyun Kim, J. Gyu Lee, H. Keun Lee, and C. Gook Park, "GPS/INS/Seeker Integrated Navigation System for the Case of GPS Blockage," 2006.
- [4] Y. Zhang, K. Kou, Y. Chen, and X. Wang, "Vision aided INS error estimation based on EKF for cruise missile," in CSAE 2012 - Proceedings, 2012 IEEE International Conference on Computer Science and Automation Engineering, 2012, vol. 1, pp. 251–254.
- [5] J. Zhao, D. J. Feng, W. M. Zhang, and W. Wang, "Inertial Navigation System Aiding by Passive Seeker Angle Tracking," in 2012 IEEE International Conference on Signal Processing, Communications and Computing, ICSPCC 2012, 2012, pp. 644–649.
- [6] G. M. Siouris, *Missile Guidance and Control Systems*. New York, NY: Springer, 2004
- [7] Veth, Michael J., "Fusion of Imaging and Inertial Sensors for Navigation" (2006). Thesis and Dissertations. 3338.
- [8] P. D. Groves, *Principles of GNSS, Inertial, and Multisensor Integrated Navigation Systems*, Second Edition. Artech House, 2013.
- [9] C.-F. Lin, *Modem Navigation, Guidance, and Control Processing*. Englewood Cliffs, N.J: Prentice Hall, 1991.

- [10] K. Ogata, *Modern Control Engineering*, 4th ed. Prentice-Hall, Upper Saddle River, NJ, 2010.
- [11] F. M. Ham and R. G. Brown, "Observability, Eigenvalues, and Kalman Filtering," in *IEEE Transactions on Aerospace and Electronic Systems*, vol. AES-19, no. 2, pp. 269-273, March 1983, doi: 10.1109/TAES.1983.309446.
- [12] S. K. Güvenç, "Range To-Go Estimation for A Tactical Missile with A Passive Seeker A Thesis Submitted To The Graduate school Of Natural And Applied Sciences Of The Middle East Technical University," 2015.
- [13] M. J. Tahk, H. Ryu, and E. J. Song, "Observability characteristics of angle-only measurement under proportional navigation," in *Proceedings of the SICE Annual Conference*, 1995, pp. 1509–1514.
- [14] M. K. Ozgoren, *Kinematics of General Spatial Mechanical Systems*. John Wiley & Sons, 2020.
- [15] B. Etkin, *Dynamics of atmospheric flight*. Dover Publications, 2005.
- [16] D. Simon. *Optimal State Estimation: Kalman, H Infinity, and Nonlinear Approaches*. Wiley-Interscience, 2006.
- [17] P. Zarchan. *Fundamentals of Kalman Filtering: A Practical Approach*. Progress In Astronautics and Aeronautics, 2009.
- [18] Maybeck, Peter S. *Stochastic Models Estimation and Control, Vol I*. Academic Press, Inc., Orlando, Florida 32887, 1979.
- [19] Tekin, R., and Erer, K. S., "Three-Dimensional Formation Guidance with Rigidly Connected Virtual Leaders", *Journal of Guidance, Control, and Dynamics*, Vol. 44, No. 6, 2021, pp. 1229-1236.
- [20] Lu, Ping, "What is Guidance?", *Journal of Guidance, Control, And Dynamics*, Vol. 44, No.7, July 2021.

- [21] Zarchan, P., *Tactical and Strategic Missile Guidance*, 7th ed., AIAA, Reston, VA, 2019, Vol. 1: pp. 45–46; Vol. 2: pp. 375–407, 412–416, 526–535.
- [22] Shukla, U. S., and Mahapatra, P. R., “The Proportional Navigation Dilemma—Pure or True?”, *IEEE Transactions on Aerospace and Electronic Systems*, Vol. 26, No. 2, 1990, pp. 382–392.
- [23] Shneydor, N. A., *Missile Guidance and Pursuit*. Horwood, Chichester, West Sussex, 1998.
- [24] Product Datasheet - Model 2443H-HR Three-Axis Hydraulic Flight Motion Simulator (FMS), downloaded on December 29, 2021, published at https://www.ideal-aerosmith.com/wp-content/uploads/2017/08/Ideal-Aero-2443H-HR_Three-Axis-Flight-Motion-Simulator_Data-Sheet_-Rev-B.pdf
- [25] Product Datasheet - 5-Axis Flight Motion Simulator HD55H-S35.70, downloaded on December 29, 2021, published at https://www.target.com.tr/wp-content/uploads/2019/06/Datasheet_5_Axis_Flight_Motion_Simulator_HD55H_S35_70.pdf
- [26] N.F. Palumbo. “Guest Editor’s Introduction: Homing Missile Guidance and Control”, *John Hopkins APL Technical Digest*, Vol. 29, No.1, 2010.
- [27] C. E. Cole Jr. “Missile Communication Links”, *John Hopkins APL Technical Digest*, Vol. 28, No.4, 2010.
- [28] Q. Wen, Q. Xia, “A Bank-to-Turn Command Calculation and Singularity Control Strategy for Agile Missiles.” In *Proceedings of the Institution of Mechanical Engineers, Part G: Journal of Aerospace Engineering* 228, no. 10, 2014, pp. 1713–1724.
- [29] G. Jang, H. Hyung, and J. Young, "Guidance performance analysis of bank-to-turn (BTT) missiles," in *Proceedings of the 1999 IEEE International Conference on Control Applications*, 1999, pp. 991-996 vol. 2.

- [30] D. Goshen and I.Y. Bar-Itzhack, "Unified Approach to Inertial Navigation System Error Modeling," *Journal of Guidance, Control and Dynamics*, vol.15, pp. 365-372, 1992.
- [31] Federal Aviation Administration, *Aeronautical Information Manual, Navigation Aid*, last visited on February 28, 2022, https://www.faa.gov/air_traffic/publications/atpubs/aim_html/chap1_section_1.html
- [32] C. Zhao, M. Kou and J. Wu, "Task allocation for integrated tactical data links," 2012 IEEE/AIAA 31st Digital Avionics Systems Conference (DASC), 2012, pp. 5E4-1-5E4-7, doi: 10.1109/DASC.2012.6382377.
- [33] K. Roessig, D. Stednitz, S. Amoroso, R. Budd and C. Laffey. "Test and Evaluation of Tactical Datalinks," AIAA 2008-1672. 2008 U.S. Air Force T&E Days. February 2008.

APPENDICES

A. Extended Kalman Filter

Linear-conventional Kalman Filter (KF) is a recursive and optimal estimation algorithm [18]. The algorithm aims to estimate the solution to a linear stochastic differential equation. However, Extended Kalman Filter (EKF) idea comes from that conventional Kalman Filter can be applied to nonlinear systems when the system is linearized around the state estimate of the filter at each epoch [8] [16].

The nonlinear discrete system and measurement model can be expressed in the following form.

$$\begin{aligned}\bar{x}_k &= f[\bar{x}_{k-1}, \bar{u}_k, \bar{w}_k] \\ \bar{z}_k &= h[\bar{x}_{k-1}, \bar{v}_k]\end{aligned}\tag{A.1}$$

where \bar{x}_k is the state vector, \bar{z}_k is the measurement vector, and \bar{u}_k is the input vector. \bar{w}_k and \bar{v}_k are assumed to be uncorrelated, zero-mean, Gaussian noises with covariance matrices, \hat{Q}_k , and \hat{R}_k , respectively.

Perturbation methods can be applied to approximate the system about nominal states. This yields linear equations, which can be solved by conventional Kalman Filter propagation and update equations [16].

EKF algorithm is summarized in Table A-1. As indicated in the table, EKF consists of two main stages, which are time propagation and the measurement update [8] [16] [17].

Table A- 1 Brief algorithm of EKF

<p>Time Propagation</p> $\bar{x}_{k+1/k} = f(\bar{x}_{k/k}, \bar{u}_k, \bar{w}_k)$ $\hat{P}_{k+1/k} = \hat{\Phi}_k \hat{P}_{k/k} \hat{\Phi}_k^T + \hat{Q}_k$ <p>Measurement Update</p> $\hat{K}_k = \hat{P}_{k+1/k} \hat{H}_k^T [\hat{H}_k \hat{P}_{k+1/k} \hat{H}_k^T + \hat{R}_k]^{-1}$ $\bar{x}_{k+1/k+1} = \bar{x}_{k+1/k} + \hat{K}_k [\bar{z}_k - h[\bar{x}_{k+1/k}]]$ $\hat{P}_{k+1/k+1} = (\hat{I} - \hat{K}_k \hat{H}_k) \hat{P}_{k+1/k}$
--

where \hat{H}_k and $\hat{\Phi}_k$ are Jacobians of h and f , respectively. $\bar{x}_{k+1/k+1}$ is the state estimate of the EKF when the measurement signal is available. $\bar{x}_{k+1/k}$ is the estimate of the EKF when there is no measurement, and states are propagated in terms of system equations. $\hat{P}_{k+1/k}$ is called as prediction covariance matrix and defines the uncertainty in the estimated state vector. The prediction covariance matrix does not depend on the measurement, as shown in Table A-1.

Kalman gain matrix, \hat{K}_k , determines the amount of the innovation term that should be included. Large \hat{K}_k values indicate that measurements affect the state's correction more. A larger Kalman gain matrix gives faster convergence but is less robust to measurement noises.

B. 4-DOF Simulation

A vector, the derivative of the vector, and the rotation of the vector have the following relationship [19]

$$\vec{\omega} = \frac{\vec{\rho} \times D_o\vec{\rho}}{\rho^2} \quad (B.1)$$

Eq. (B.1) can also be seen in Figure B-1. The derivation details of Eq. (B.1) are given in [19].

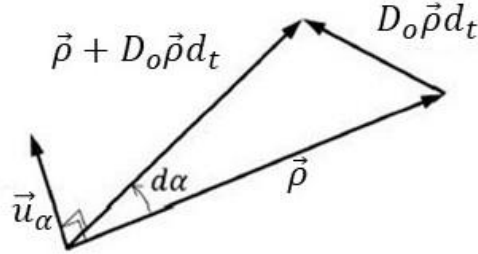


Figure B-1 vector, the derivative of the vector, and rotation vector relations [19]

4-DOF simulation is an application of Eq. (B.1). If the vector is chosen as the velocity vector, \vec{v}_B , angular velocity of \vec{v}_B , becomes

$$\vec{\omega}_B = \frac{\vec{v}_B \times \vec{a}_B}{v_B^2} \quad (B.2)$$

Assuming the body frame coincides with the velocity frame, angular velocity of \vec{v}_B is the same as the body's angular velocity. So that, Eq. (B.2) becomes as

$$\vec{\omega}_B^{(b)} = \begin{bmatrix} p \\ q \\ r \end{bmatrix} = \frac{\tilde{v}_B^{(b)} \vec{a}_B^{(b)}}{v_B^2} \quad (B.3)$$

where $\vec{\omega}_B^{(b)}$ body angular rates. Since the body frame coincides with the velocity frame, the velocity vector can be resolved in the body frame as follows

$$\bar{v}_B^{(b)} = [V \ 0 \ 0]^T \quad (B.4)$$

As shown from Figure B-1 and Eq. (B.4), the first component of the angular velocity vector resolved in the body frame is redundant and can be used as the designer's needs [19]. In [19], proportional control is an example of keeping roll angle at zero.

In the 4-DOF simulation, the missile's position and velocity are obtained by integrating the acceleration command produced by the guidance. In addition, the angular position is obtained by using Eq. (B.3) in the following equation.

$$\dot{\hat{C}}^{(i,b)} = \hat{C}^{(i,b)} \tilde{\omega}_B^{(b)} \quad (B.5)$$

where $\hat{C}^{(i,b)}$ is the transformation matrix from the body to the inertial frame. By integrating Eq. (B.5), $\hat{C}^{(i,b)}$ can be obtained, and euler angles can be obtained from DCM as follows [14], [8]

$$\begin{aligned} \phi &= \text{atan}_2 \left(\hat{C}^{(i,b)}(3,2), \hat{C}^{(i,b)}(3,3) \right) \\ \theta &= -\text{asin} \left(\hat{C}^{(i,b)}(3,1) \right) \\ \psi &= \text{atan}_2 \left(\hat{C}^{(i,b)}(2,1), \hat{C}^{(i,b)}(1,1) \right) \end{aligned} \quad (B.6)$$

The following figures show the models used in the simulation. Figure B-2 shows that the missile's position and velocity are obtained from integrating acceleration, which is calculated by the guidance law. Figure B-3 shows how Eq. (B.5) and Eq. (B.6) are handled in the simulation. Finally, Figure B-4 shows how Eq. (B.3), the core of the 4-DOF simulation, is modeled. The BTTEnable parameter is used to decide whether the missile flies on Skid-to-Turn (STT) mode or Bank-to-Turn (BTT) mode. If the BTTEnable is 1, p is calculated by Eq. (4.5); otherwise, p is calculated by Eq. (4.3).

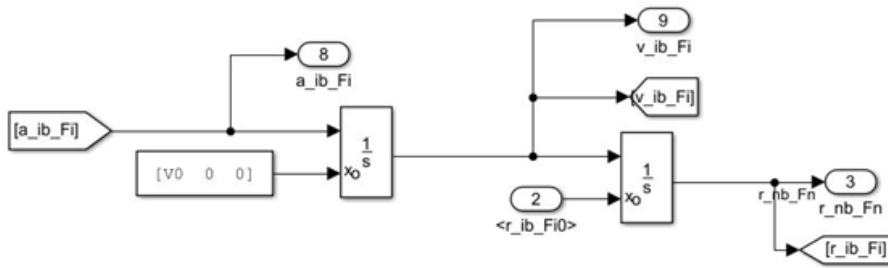


Figure B-2 Integrating acceleration to obtain velocity and position

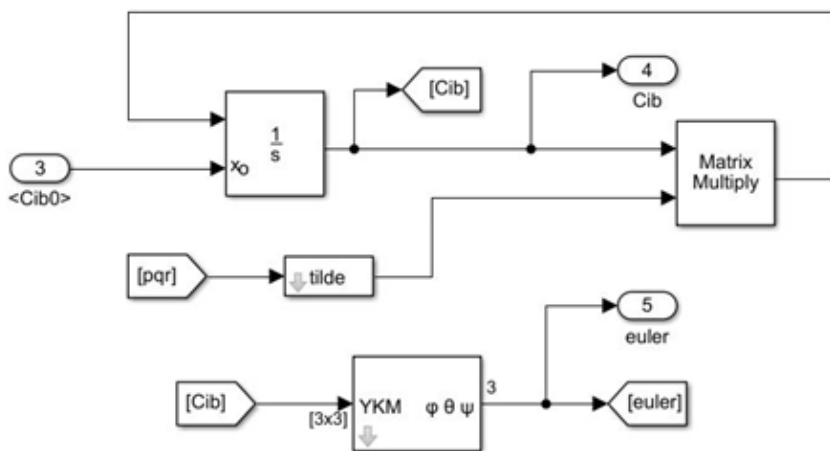


Figure B-3 DCM integration and obtaining Euler angles from DCM
(Eq. (B.5) and Eq. (B.6))

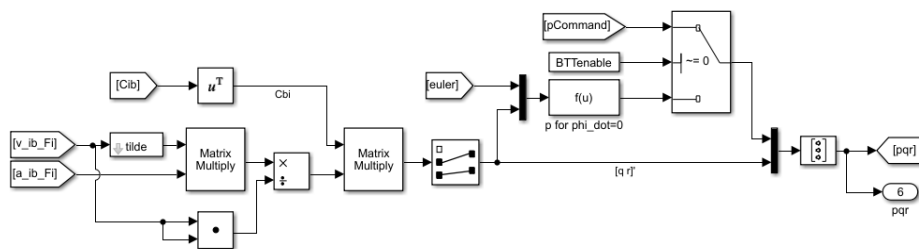


Figure B-4 Simulink model of Eq. (B.3)

C. Instrument Models

In this part, Accelerometer, seeker, and datalink measurement models, which are the primary sensors integrated in this thesis, are given.

Accelerometer Model

Accelerometers measure specific-force, the difference between the acceleration relative to the inertial frame and the gravitation. Specific-force can be defined as

$$\vec{f} = \vec{a} - \vec{g} \quad (C.1)$$

where \vec{f} is the specific-force, \vec{a} is the acceleration vector, and \vec{g} is the gravitation vector.

Error sources corrupt the accelerometer outputs. Most encountered errors are as follows:

Bias: a bias is a constant or slowly-varying additive error. It can change with every use of the accelerometer or the temperature changing. By most authors, \vec{b}_a is used for acceleration bias [8].

Scale Factor: a scale factor error is a constant or slowly-varying multiplicative error. By most authors, \hat{S}_a is used for the acceleration scale factor [8].

Misalignment: it is the result of mechanical fabrication and installation errors. Misalignment errors differentiate between the accelerometers' sensitive axes and the platform reference. Misalignment and the scale factor errors are denoted by a single matrix, whose diagonal elements are of scale factor, and non-diagonal elements are of misalignment. Scale factor and the misalignment errors are unitless, and they are expressed in ppm (parts per million) or as a percentage [8].

Random Noise: it is an additive error with high-bandwidth power spectral density (PSD). The random noise is denoted w_a for accelerometers. The units are $\mu\text{g}/\sqrt{\text{hr}}$ for

accelerometer random noise [8]. Random noise cannot be calibrated or compensated because there is no correlation between past and future values.

The accelerometer measurements can be modeled with the errors as follows

$$\bar{f}_{ib}^{(b)'} = \bar{b}_a^{(b)} + (\hat{I}_{3 \times 3} + \hat{M}_{a_{3 \times 3}})\bar{f}_{ib}^{(b)} + \bar{w}_a^{(b)} \quad (C.2)$$

where $\bar{f}_{ib}^{(b)'}$ is the output of the accelerometer, and $\bar{f}_{ib}^{(b)}$ is the true values. In this study, only constant bias and uncorrelated, zero-mean additive Gaussian noise where $w_a \sim N(0, \sigma_a)$ are used as error sources.

Seeker Measurements

As shown in Figure C-1, the seeker is generally categorized with three types: active, semi-active or passive. Active seekers self-illuminate the target. Since the seeker transmits the energy to the target, the target can detect and track the missile. In semi-active seekers, the target is illuminated by the platform or the adjacent location. Instead of illuminating the target, Passive seekers detect and track energy emanating from the target [26]. Infrared (IR), imaging infrared (IIR), and radio-frequency (RF) seekers are common types of passive seekers used in tactical missiles. In these study, a gimballed IIR seeker is considered.

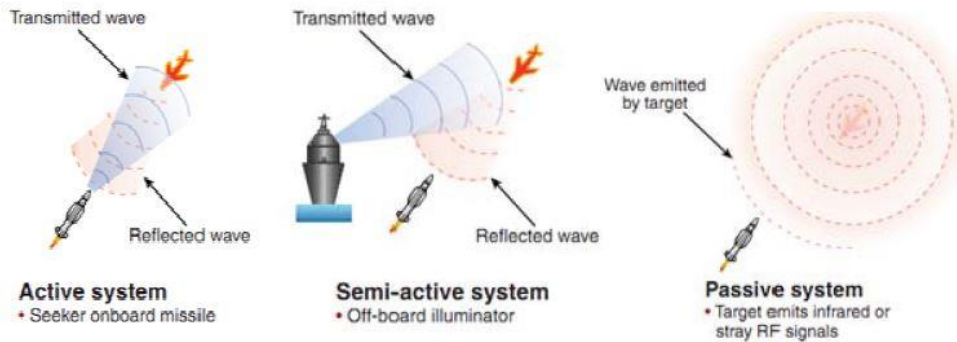


Figure C-1 Seeker types [26]

Gimbaled seekers can have encoders and gyros on themselves. Encoders can measure the angular deflection of the seeker gimbal, while seeker gyros measure the angular rates of the seeker gimbal. In this study, encoder outputs are used as seeker measurements. Also, it is assumed that seeker measurement has only uncorrelated, zero-mean additive Gaussian noise, which is mainly caused by the quantization.

In this study, the seeker has a two-axis gimbal system that consists of pitch rotation for the inner gimbal, and yaw rotation for the outer gimbal, as shown in Figure C-2.

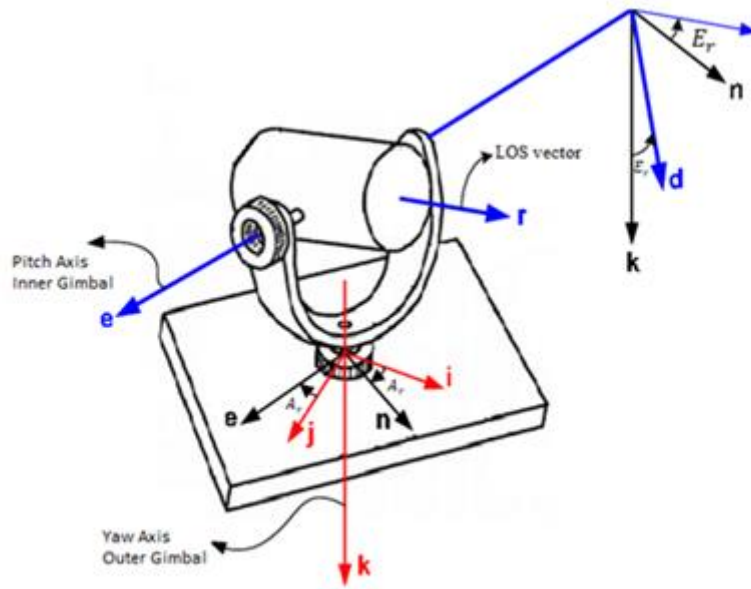


Figure C-2 Seeker and corresponding successive rotation angles

LOS angles are defined as follows

$$\lambda_{az} = \tan^{-1} \left(\frac{y_{mL}}{x_{mL}} \right) + \eta_\lambda \quad (C.3)$$

$$\lambda_{el} = -\tan^{-1} \left(\frac{z_{mL}}{\sqrt{x_{mL}^2 + y_{mL}^2}} \right) + \eta_\lambda \quad (C.4)$$

where λ_{az} and λ_{el} are yaw and pitch angle measurements, respectively. x_{mL}, y_{mL}, z_{mL} are LOS vector elements from missile to landmark, and η_λ is an uncorrelated, zero mean additive Gaussian noise where $\eta_\lambda \sim N(0, \sigma_\lambda)$.

Datalink Measurement

Datalink is used for signal transmission and emission. However, datalink can supply range and range rate information between transmitter and emitter. In this study, only the range information is used as data link measurement.

The range can be measured by measuring the signal's flight time or estimated from the received signal strength [8]. The accuracy of the range is limited by the clock resolution. Also, RF noise can result in random noise error to the system. There are two major contributors for noise: thermal noise in the receiver and jammer noise [27]. In this study, noise is modeled as an uncorrelated, zero mean additive Gaussian noise.

Datalink range measurement can be expressed in terms of positions of platform and missile as

$$r = \sqrt{(x_m - x_p)^2 + (y_m - y_p)^2 + (z_m - z_p)^2} + \eta_r \quad (C.5)$$

where x_m, y_m, z_m are the position of the missile, and x_p, y_p, z_p are the position of the platform, and η_r is an uncorrelated, zero mean additive Gaussian noise where $\eta_r \sim N(0, \sigma_r)$.

D. Guidance Laws

Guidance is the process of determining the guidance command, which steers the missile to fly a trajectory that provides the specified terminal conditions [20]. These terminal conditions can be acceptable miss-distance, pre-specified impact angle, or pre-specified time-to-go. In this study, proportional navigation guidance (PNG) and velocity pursuit are utilized as guidance laws.

PNG is well known and most used guidance law [21]. PNG is the optimal guidance law in the sense of minimizing miss-distance for aerodynamically controlled missiles. There are two versions of the PNG, which are true PNG (TPN), and pure PNG (PPN). In TPN, acceleration command is produced perpendicular to LOS vector, whereas PPN produces acceleration command perpendicular to velocity vector [22]. PNG is a P-controller, which aims to diminish error term, LOS rate, in this case, to control missile acceleration. This phenomenon has been known by the mariners for centuries. Keeping the LOS vector's direction constant in the inertial space guarantees collision [23]. For aerodynamically controlled missiles, controlling velocity along the x-direction is not possible. Hence, in this study, PPN is used.

The acceleration command produced by the PNG is as follows [21]:

$$\vec{a}_b = N \frac{\vec{r}_{bt} \times \vec{v}_c}{r_{bt}^2} \times \vec{v}_b \quad (D.1)$$

where \vec{r}_{bt} is the LOS vector, \vec{v}_c is the closing velocity, \vec{v}_b is the missile velocity, and N is the navigation gain.

For stationary target, closing velocity can be taken as the minus of the missile velocity.

Another guidance law used in this study is velocity pursuit. Velocity pursuit requires missile velocity to coincide with the LOS vector [23]. Collision is guaranteed when the velocity vector and LOS vector overlaps and are kept. Since the missile moves along the LOS vector, the LOS vector direction is constant, and the LOS rate is zero.

The acceleration command produced by the velocity pursuit is as follows:

$$\vec{a}_b = K(\vec{u}_v \times \vec{u}_r) \times \vec{v}_b \quad (D.2)$$

where \vec{u}_v is the unit vector of the missile velocity vector, \vec{u}_r is the unit vector of the LOS vector, and K is the control gain that determines the rate of convergence.

E. Investigating the Observability of “Case 2” and “Case 3”

The observability of the states of Section 2.2 is investigated here. However, before going further, Kalman Filter observability should be reviewed. There are two types of observability definitions for the KF [8]. The first definition is called as deterministic observability, or geometric observability, which expresses if there is sufficient measurement information to estimate all states in the absence of noise. The second definition is called stochastic observability, which is about the rate of convergence of the KF. Stochastic observability depends on the measurement noise, level of system noise, and measurement sampling time [8]. To determine stochastic observability, a normalized process error covariance matrix is calculated at every epoch. Since the process covariance matrix is related to uncertainties, stochastic observability can be said not to be directly related to the observability of the states but the rate of convergence of the states.

At the single epoch of the measurement, Kalman Filter can estimate the states that are directly related to the measurements. The other states can be estimated by the time-dependent relationship between observable states through the system transition matrix, $\hat{\Phi}_k$ [8].

The linear or linearized Kalman Filter is defined as

$$\begin{aligned}\bar{X}_k &= \hat{\Phi}_{k-1} \bar{X}_{k-1} + \hat{G}_{k-1} \bar{W}_{s,k-1} \\ \bar{Z}_k &= \hat{H}_k \bar{X}_k + \bar{W}_{m,k}\end{aligned}\tag{E.1}$$

In the sense of deterministic observability, to determine whether the states are fully observable or not, the observability matrix, $\hat{O}_{1:k}$'s rank is checked. If the rank of the observability matrix is equal to the number of states, it is called as fully observable. The observability matrix is defined as [8]

$$\hat{O}_{1:k} = \begin{bmatrix} \hat{H}_1 \\ \hat{H}_2 \hat{\Phi}_1 \\ \vdots \\ \hat{H}_k \hat{\Phi}_{k-1} \dots \hat{\Phi}_2 \hat{\Phi}_1 \end{bmatrix} \quad (E.2)$$

the observability matrix of KF is somehow similar to the observability matrix of the unforced continuous systems, as it is defined as

$$\begin{aligned} \dot{\bar{X}} &= \hat{A}\bar{X} \\ \bar{y} &= \hat{C}\bar{X} \end{aligned} \quad (E.3)$$

To determine whether the system is fully observable or not, the observability matrix, \hat{O} , is analyzed. When the rank of the observability matrix is equal to the number of the states, the system is called fully observable [10].

$$\hat{O} = \begin{bmatrix} \hat{C} \\ \hat{C}\hat{A} \\ \vdots \\ \hat{C}\hat{A}^{n-1} \end{bmatrix} \quad (E.4)$$

Another observability analysis method is stochastic observability. In this analysis, eigenvalues of the normalized prediction covariance matrix, \hat{P}'_k , are calculated [11]. For this purpose, the error covariance matrix is normalized first by using the following equation

$$\hat{P}'_k = \left(\sqrt{\hat{P}_0} \right)^{-1} \cdot \hat{P}_k \cdot \left(\sqrt{\hat{P}_0} \right)^{-1} \quad (E.5)$$

After Eq. (2.17) is applied, the normalized covariance matrix is bounded by multiplying $\frac{n}{Tr(\hat{P}'_k)}$ [11], where Tr indicates the trace of the matrix, which is the sum of the diagonal elements, and n is the number of states. The eigenvalues are bounded between 0 and n by this multiplication.

$$\hat{P}_k^N = \frac{n}{Tr(\hat{P}'_k)} \hat{P}'_k \quad (E.6)$$

Eigenvalues of the \hat{P}_k^N give information about the observability of the corresponding states. Low-valued eigenvalues indicate more observability for the corresponding state [11].

Deterministic observability gives the information of the number of observable states. Stochastic observability gives the rate of convergence of the states. Considering both methods simultaneously provides more insight into the observability of the Kalman Filter. However, one should keep that in mind; finding corresponding eigenvalues for a system having many states would be tiresome.

As it can be seen from Eq. (E.2) and Eq. (E.6), to analyze the observability of the system, simulation should be run, and the \hat{P}_k , \hat{H}_k and $\hat{\Phi}_k$ matrices should be extracted from the simulation to check whether the Kalman Filter is observable or not.

In [2], the observability issue is considered in terms of the observability matrix, which is the deterministic observability approach. In this thesis, the same deterministic observability approach is applied. After the simulation is run, the observability matrix is obtained by Eq. (E.2), and the rank of the observability matrix is found as 6, which means all states are observable.

The observability matrix is also obtained for Case 3, and the rank of the observability matrix is found as 8, which indicates that proposed method is also observable.

At that point, it can be utilized that range-to-go estimation and target motion analysis (TMA) with a passive seeker suffer from observability issues as well [12] [13]. Even though the two problems are not identical, there is an analogy. If the position error of the missile is compensated by using LOS angles with a known landmark, the range between the missile and the landmark can also be estimated by these data. The difference between our problem and the TMA is that in our problem, landmark position is assumed to be known, whereas in the TMA problem missile's position is known [13]. [13] shows that observability can be assured if the LOS rate is nonzero.

As mentioned before, when there is no LOS rate, the LOS angle from missile to landmark is not sufficient to analyze the motion of the missile. To test this phenomenon, following scenario is conducted.

In this scenario, the missile approaches the landmark by using velocity pursuit as guidance law. As indicated in Appendix D, velocity pursuit guidance law produces acceleration command so that the missile velocity vector rapidly coincides with the LOS vector, resulting in zero LOS rate.

The results of the scenario are given below. Figure E-1 shows the trajectory of the missile and LOS angle. Since velocity pursuit is used, missile's velocity coincides with the LOS vector, which keeps the LOS angle constant and LOS rate at zero, as seen from the bottom figure. Figure E-2, Figure E-3, and Figure E-4 show the position, velocity, and bias errors estimated by the filter. At the beginning of the simulation, errors are compensated since there is a LOS rate, as seen from the bottom figure of Figure E-1. However, the filter cannot estimate errors when the LOS rate is zero as it is expected.

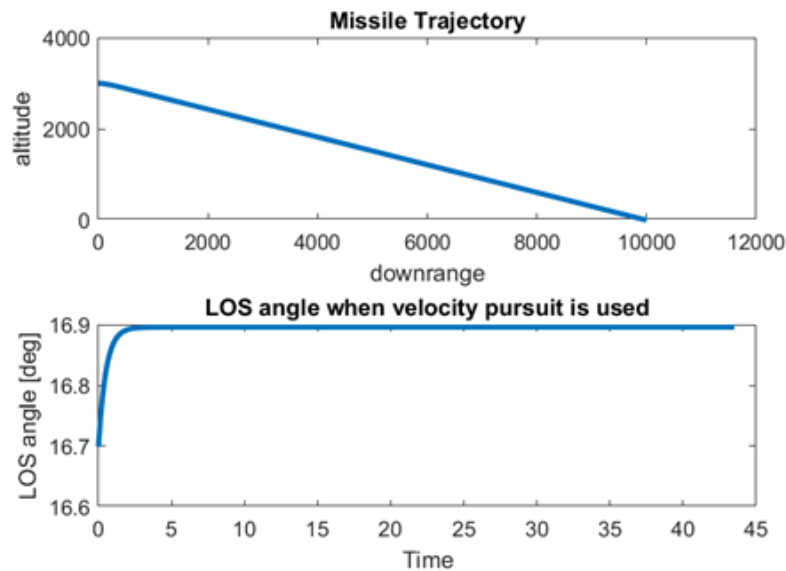


Figure E-1 Trajectory of the missile and LOS angle when velocity pursuit is used to approach the landmark

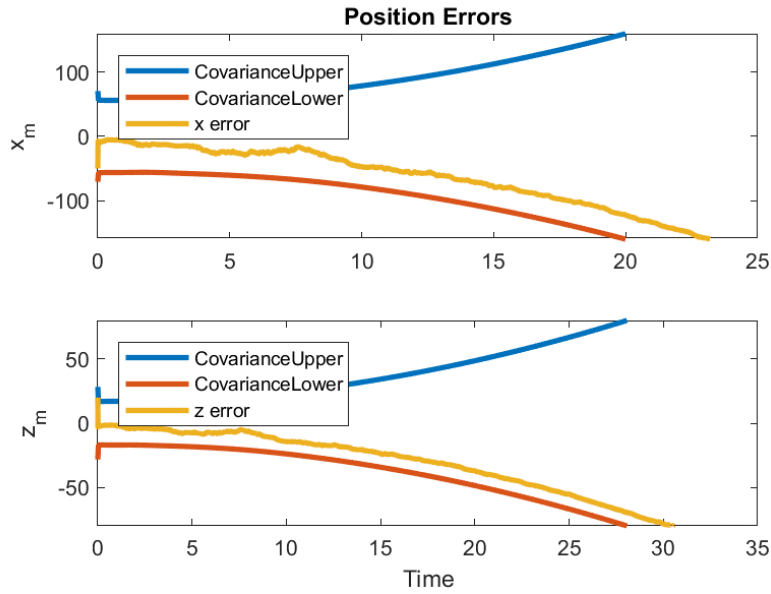


Figure E-2 Position errors when velocity pursuit is used to approach the landmark

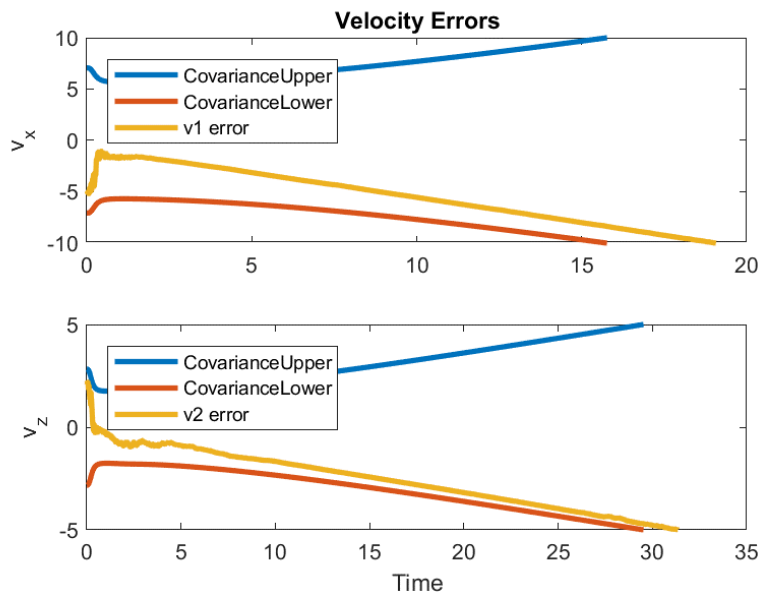


Figure E-3 Velocity errors when velocity pursuit is used to approach the landmark

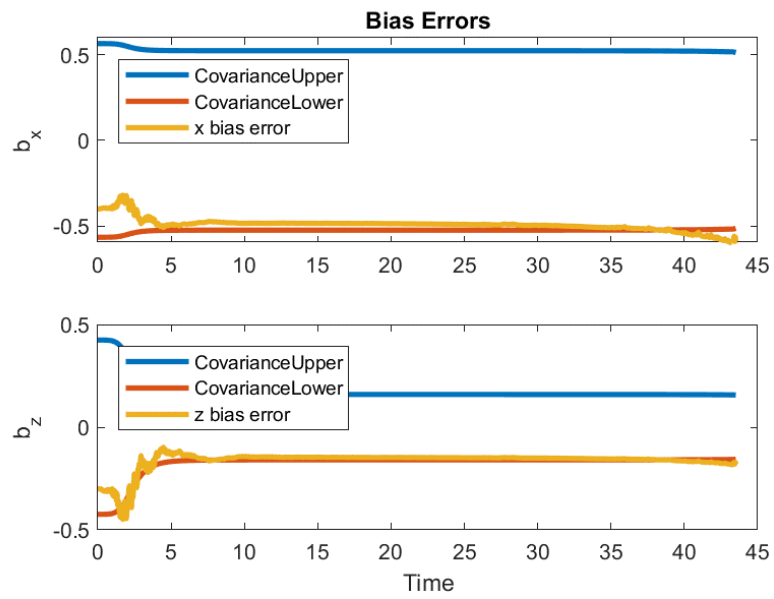


Figure E-4 Bias Errors when velocity pursuit is used to approach the landmark